REPORT DOCUMENTATION PAGE

Form Approved
OMB No. 0704-0188

1. REPORT DATE *(DD-MM-YYYY)*	**2. REPORT TYPE**	**3. DATES COVERED** *(From - To)*
June 2014	Technical Paper	June 2014- July 2014

4. TITLE AND SUBTITLE

Low-Voltage Hall Thruster Mode Transitions

5a. CONTRACT NUMBER
In-House

5b. GRANT NUMBER

5c. PROGRAM ELEMENT NUMBER

6. AUTHOR(S)

Brown, D. L., Lobbia, R. B., Blakely, J. M.

5d. PROJECT NUMBER

5e. TASK NUMBER

5f. WORK UNIT NUMBER
Q18A

7. PERFORMING ORGANIZATION NAME(S) AND ADDRESS(ES)

Air Force Research Laboratory (AFMC)
AFRL/RQRS
1 Ara Drive.
Edwards AFB CA 93524-7013

8. PERFORMING ORGANIZATION REPORT NO.

9. SPONSORING / MONITORING AGENCY NAME(S) AND ADDRESS(ES)
Air Force Research Laboratory (AFMC)
AFRL/RQR
5 Pollux Drive
Edwards AFB CA 93524-7048

10. SPONSOR/MONITOR'S ACRONYM(S)

11. SPONSOR/MONITOR'S REPORT NUMBER(S)
AFRL-RQ-ED-TP-2014-198

12. DISTRIBUTION / AVAILABILITY STATEMENT
Distribution A: Approved for Public Release; Distribution Unlimited

13. SUPPLEMENTARY NOTES
Technical paper presented at 50th AIAA/ASME/SAE/ASEE Joint Propulsion Conference, Cleveland, OH, 28-30 July, 2014.
PA#14356

14. ABSTRACT
Past investigations of the 6kW-class H6 Hall thruster during low-voltage operation revealed two operating modes, corresponding to the presence or absence of azimuthal propagating plasma spokes. The modes exhibited differences in thruster performance and plume properties, including electron current to the anode that varied by up to 10% of the discharge current between operating modes. New evidence is presented that provides insight into the transition between operating modes, including hysteresis and the impact of cathode location. Global maps of thruster stability were examined, including maps of thruster current-voltage-magnetic field (I-V-B) and variation in cathode to ground potential for the IV-B surface. These I-V-B topologies were characterized for the H6 Hall thruster from 100V to 200V discharge, with variation in cathode flow fraction, cathode position inside and outside the magnetic field seperatrix, asymmetric magnetic field, and anode flow rate. Results indicate different plasma processes may trigger the transition to a highly oscillatory, global operational mode at reduced discharge voltage and low magnetic field strength. The transition at low magnetic field is insensitive to variation in cathode flow and cathode configuration, and occurs at a constant magnetic field for discharge voltage greater than 130V. The transition at low voltage is influenced by cathode flow fraction, cathode configuration, and anode flow rate. Possible mechanisms are considered, including the electron gyroradius and electron mobility.

15. SUBJECT TERMS

16. SECURITY CLASSIFICATION OF:			**17. LIMITATION OF ABSTRACT**	**18. NUMBER OF PAGES**	**19a. NAME OF RESPONSIBLE PERSON**
					D. Brown
a. REPORT	**b. ABSTRACT**	**c. THIS PAGE**	SAR	41	**19b. TELEPHONE NO** *(include area code)*
Unclassified	**Unclassified**	**Unclassified**			661-275-5028

Standard Form 298 (Rev. 8-98)
Prescribed by ANSI Std. 239.18

Low-Voltage Hall Thruster Mode Transitions

Daniel L. Brown [1]
U.S. Air Force Research Laboratory, Edwards AFB, CA, 93524, USA

and

Robert B. Lobbia [2], Joseph M. Blakely[3]
ERC Inc., Edwards AFB, CA, 93524, USA

Past investigations of the 6kW-class H6 Hall thruster during low-voltage operation revealed two operating modes, corresponding to the presence or absence of azimuthal propagating plasma spokes. The modes exhibited differences in thruster performance and plume properties, including electron current to the anode that varied by up to 10% of the discharge current between operating modes. New evidence is presented that provides insight into the transition between operating modes, including hysteresis and the impact of cathode location. Global maps of thruster stability were examined, including maps of thruster current-voltage-magnetic field (I-V-B) and variation in cathode to ground potential for the I-V-B surface. These I-V-B topologies were characterized for the H6 Hall thruster from 100V to 200V discharge, with variation in cathode flow fraction, cathode position inside and outside the magnetic field seperatrix, asymmetric magnetic field, and anode flow rate. Results indicate different plasma processes may trigger the transition to a highly oscillatory, global operational mode at reduced discharge voltage and low magnetic field strength. The transition at low magnetic field is insensitive to variation in cathode flow and cathode configuration, and occurs at a constant magnetic field for discharge voltage greater than 130V. The transition at low voltage is influenced by cathode flow fraction, cathode configuration, and anode flow rate. Possible mechanisms are considered, including the electron gyroradius and electron mobility.

Nomenclature

e	=	elementary charge (1.602×10^{-19} C)
k	=	Boltzmann constant (1.3807×10^{-23} J/K)
m_e	=	electron mass (9.109×10^{-31} kg)
r_e	=	electron gyroradius
T_e	=	electron temperature
$\mu_{e\perp}$	=	cross-field electron mobility
υ_e	=	total effective electron collision frequency
Ω_e	=	electron Hall parameter

[1] Program Manager, In-Space Propulsion Branch, Aerospace Systems Directorate (AFRL/RQRS), daniel.brown.50@us.af.mil, Member AIAA.
[2] Senior Scientist, In-Space Propulsion Branch, Aerospace Systems Directorate (AFRL/RQRS), robert.lobbia.ctr@us.af.mil.
[3] Research Scientist, now with First Solar, Inc.

I. Introduction

EARLY investigations in the former Soviet Union observed and characterized Hall thruster discharge oscillations, which are considered an inherent process associated with Hall thruster technology.[1,2] The oscillations are often related to ionization instabilities and density gradients that are dependent on the thruster operation, including variations in discharge voltage, anode propellant mass flow rate, cathode location and propellant flow rate, propellant type, thruster geometry, power-processing unit (PPU) characteristics, and magnetic field strength and topography. A comprehensive overview of these Hall thruster discharge oscillations ranging from approximately 1-kHz up to over 60-MHz was described by Choueiri.[3]

Several recent investigations have studied complex fluctuations inherent in a Hall thruster discharge, and analyzed thruster operating modes dependent on the thruster operation and design. A systematic study of oscillation behavior from 2-kHz to 100-kHz detailed the influence of azimuthal density non-uniformities and probe perturbations, and revealed that the interactions of these effects with the natural Hall thruster discharge dynamics may cause instabilities.[4] A study on the BHT-1500 characterized two operating modes that were sensitive to magnetic field, termed the "jet-mode" and "collimated mode".[5] These modes were attributed to the location of ionization within the discharge channel, and exhibited variations in ion current density and ion energy distribution in the plume. Extensive studies of Hall thruster dynamics and oscillation behaviors have been conducted throughout the literature, however, the nature of these effects is extremely complex and difficult to quantify.

Past investigations of low discharge voltage behavior at AFRL with the H6 Hall thruster revealed discontinuities in thruster performance that occurred for small variations in operating parameters.[6] Minor changes in magnetic field or cathode flow rate resulted in an intense, visible transformation of the jet-mode plume structure. This transformation corresponded to an abrupt escalation in the discharge current with constant thrust and amplification of the discharge oscillations. The transition was achieved with a hysteresis effect, such that identical operation set-points may generate vastly different discharge properties. It has been well documented that low discharge voltage operation is associated with increased oscillation behavior and variation in thruster performance.[7,8] Since the specific nature of the oscillations in this study are unknown, the existence of two discharge operating regimes led to classification as the high-current mode and low-current mode.

In this paper, global maps of thruster operation were examined that provide insight into the H6 thruster behavior, including surface topologies of thruster discharge current-voltage-magnetic field (I-V-B). These I-V-B topologies were characterized from 100V to 200V discharge, with variation in cathode flow fraction (CFF), cathode position inside and outside the magnetic field seperatrix, and anode flow rate. In addition, topologies of cathode to ground potential as a function of voltage and magnetic field provide a global assessment of facility coupling. Results were evaluated in the context of past measurements of low-voltage H6 operation to develop new understanding of the thruster behavior and mode transitions. Maps of the global thruster behavior enhance assessment of hysteresis in operating modes and modes observed at higher specific impulse operation.[9,10]

II. Background

In past studies at the Air Force Research Laboratory (AFRL), low discharge voltage Hall thruster behavior revealed a large increase in the amplitude of discharge current oscillations up to ~10% in high-current mode, as shown in Fig. 1 for 10 mg/s anode flow and a center-mount cathode configuration. The regimes were characterized through a systematic mapping of low discharge voltage Hall thruster performance with variations in the applied anode-to-cathode potential, anode mass flow rate at 10, 15, and 20mg/s, and CFF from 7% up to 26% of the anode flow. In Fig. 1a, increased CFF reduced discharge current for operation from 100V to 110V, and falls to the trend from higher voltage operation. The discharge regimes were highly dependent on near-field neutral density and magnetic field topography. Since variation in thrust was minimal with increased CFF <120V, thrust to power (T/P) increased in Figs. 1c and 1d. Overall, the increasing CFF to enable low-voltage mode operation increased total efficiency.

The transition between low discharge voltage operating regimes corresponded to a sudden transformation of the jet-mode plume structure. The plume transformed from an extended, diffuse jet during high-current mode to a more compact jet located further upstream during low-current mode operation. The Hall thruster jet-mode is characterized by a visible jet-like plume profile extending several thruster diameters downstream of the exit, and is distinguished from a diffuse glow discharge by a significantly lower discharge current. Both jet-mode regimes in this study exhibited substantially lower discharge current than operation in the diffuse glow discharge mode. High resolution images of the operating regimes are shown in Fig. 2, and contours of constant image intensity more clearly show the extended plume structure in the high-current mode compared to the low-current mode. This qualitative visualization illustrates the extended plume features discernible by eye in laboratory experiments.

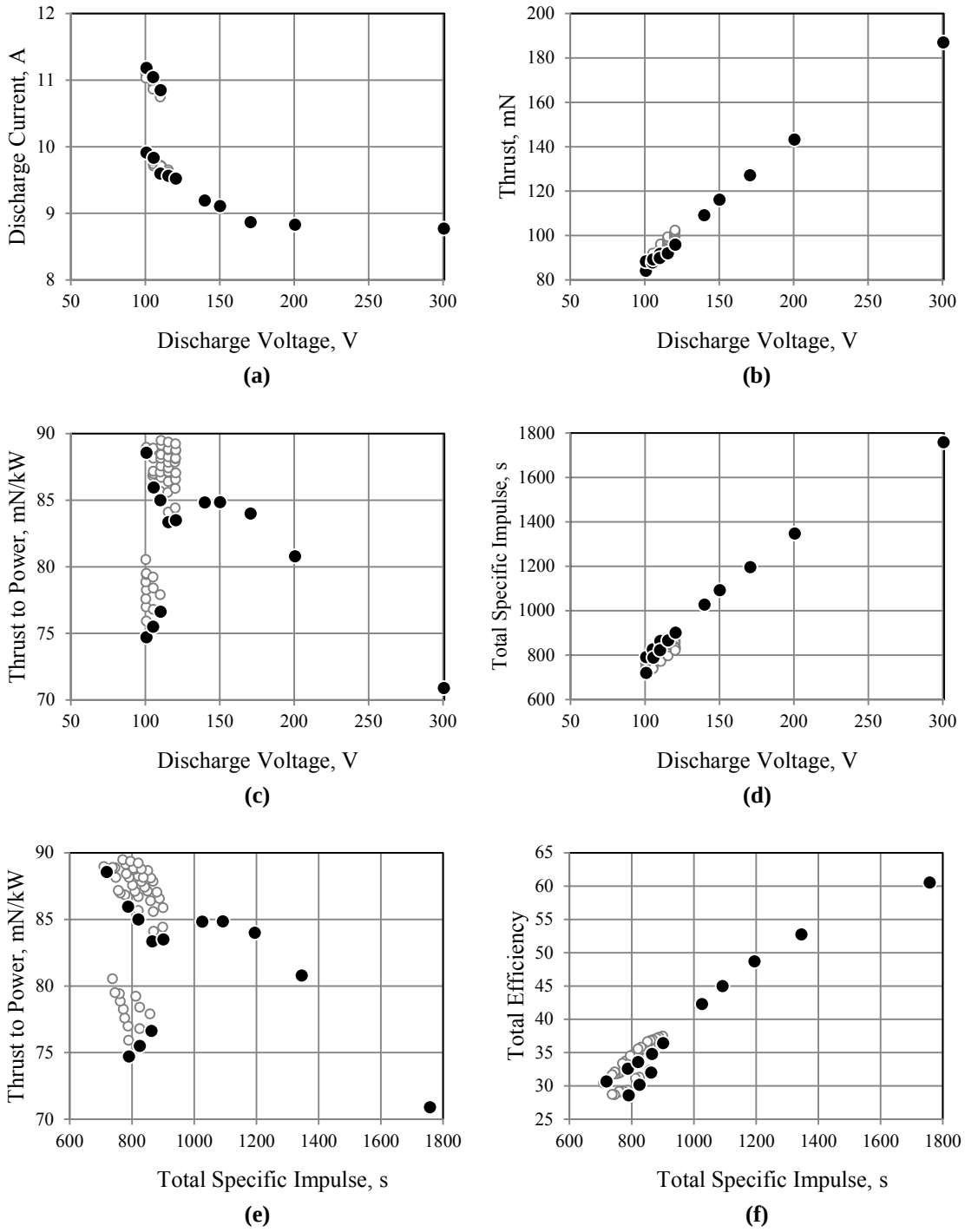

Figure 1. H6 Hall thruster low-voltage characterization at 10mg/s and variation in center-mount cathode flow for (a) discharge current, (b) thrust, (c) thrust to power ratio, (d) total specific impulse, and performance characterization as a function of total specific impulse for (e) thrust to power ratio and (f) total efficiency.[6] Solid marker are operation at 7% CFF from 100V to 300V, and at the minimum CFF for low-current mode operation from 100V to 120V. Open markers from 100V to 120V are variation in CFF ranging 8% to 26%.

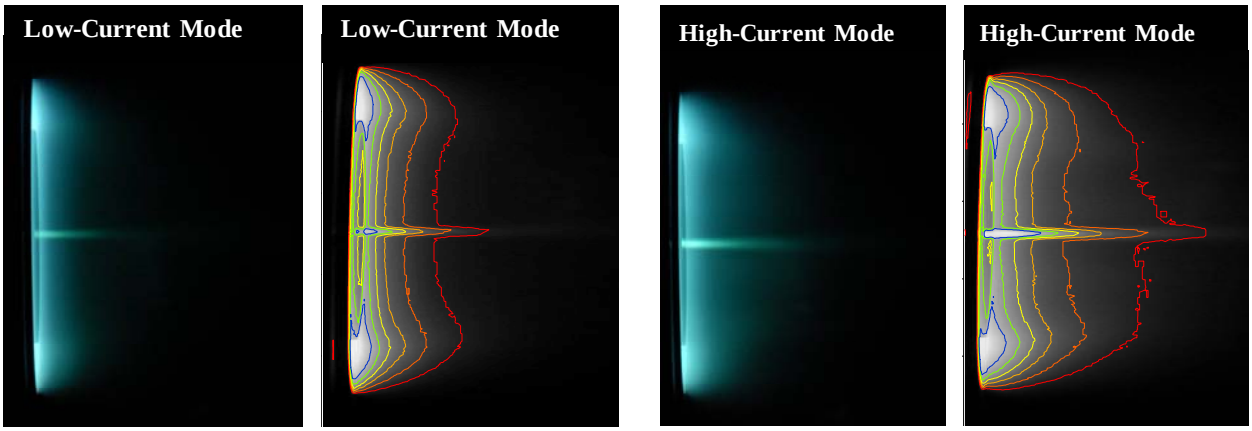

Figure 2. H6 Hall thruster jet mode plume structure for 105V, 20mg/s. Local mode, or low-current mode, is shown as (a) photograph and (b) contours of constant image intensity. Global mode, or high-current mode, is shown as (c) photograph and (d) contours of constant image intensity.[6]

During operation near the transition point between the two states, the thruster showed visible signs of flickering and instability. Performance measurements were not taken in this unstable transition regime due to uncertainties in thrust measurements for indeterminate pulsing. The thruster operated in a stable jet-mode in both the high-current and low-current states. As stated previously, the transformation between thruster operating regimes revealed characteristics of hysteresis, where a large cathode flow rate and magnetic field were required to transition from the high-current to low-current regimes. Once the transition to low-current mode occurred, the cathode flow and magnetic field could be decreased while maintaining the decreased current operation.

Evaluation of the thruster performance and far-field plume demonstrated that electron current to the anode was the primary source of increased discharge current in the high-current regime. Analysis of the ion energy distributions and ion energy per charge distributions revealed that the high-current regime corresponded to increased multiply-charged ions and wide dispersion in the ion species energy distributions. This phenomenon may be caused by the cyclic exhaust and resupply of neutral propellant in the discharge. Increased neutral flow to the near-cathode region by additional cathode flow injection, through an auxiliary port, or by increased facility background pressure was shown to enable thruster operation in the more efficient low-current mode. Follow-on studies revealed the operating regimes were associated with the presence or absence of azimuthal spoke structures in the plasma, and were present at nominal 300V discharges and above.[11] The high-current operating mode, also called "global mode" is a result of instability associated with large global axial instabilities, specifically the Hall thruster breathing mode. Low-current mode, also termed "local mode" corresponded to rotating azimuthal spoke instability. The high-current mode discharge oscillations declined with increased neutral flow near the thruster exit, and eventually enabled operation in the low-current regime. Conversely, oscillations in the high-current regime were amplified as neutral density in the near-field was decreased.

III. Experimental Apparatus

A. H6 Hall Thruster

Investigations of low discharge voltage operation were conducted with the H6, a nominal 6-kW laboratory model Hall thruster using xenon propellant. The thruster was developed at AFRL in collaboration with the Jet Propulsion Laboratory (JPL) and University of Michigan (UM) to serve as a standardized test-bed for Hall thruster physics research, and is based on the 5kW-class P5 Hall thruster and NASA-173M design heritage.[12,13,14,15.16,17] In this study, two cathodes were utilized to assess cathode location on low-voltage thruster operation. A high-current lanthanum hexaboride (LaB6) hollow cathode developed at JPL was positioned in the nominal, centrally-mounted configuration on the thruster centerline axis.[18] A Busek BHC-5000 BaO hollow cathode was positioned outside the outer pole at the 12 0'clock location and approximately 2 inches radially from the outer pole, which is comparable to past investigations. In this external configuration, the BHC-5000 cathode exit orifice was outside of the magnetic field separatrix and the axial position was equivalent to the center mount configuration. Cathode flow fraction was

typically 7% of the anode flow, unless otherwise noted. Past comparisons of Hall thruster operation using these two cathodes demonstrated consistent high performance for multiple conditions. Although differences due to cathode design or operation may contribute to thruster behavior observed in this study, the cathode location is expected to have a more significant impact.

Xenon propellant flow system was supplied with research grade xenon (99.9995% purity). Anode flow was controlled with a 1000-sccm Unit 1661 digital mass flow controller and cathode flow was regulated with a 100-sccm Unit 8161 digital mass flow controller. All mass flow controllers were calibrated with xenon prior to testing with a Mesa Labs Definer 220 series dry calibration system, with an estimated uncertainty of <1% accuracy over full range according to the manufacturer's specifications.

Thruster discharge power was provided by a 1000-V, 150-A AMREL HPS1000-150 DC power supply in-line with a low-pass filter. The filter was located outside the facility near the electrical feed-through. Separate power supplies were used for thruster electromagnets, cathode heater, and keeper. Due to the long electrical connections in the SPEF facility, typically greater than 150-ft end to end, all thruster discharge cables and telemetry wiring inside and outside the chamber were shielded with conductive conduit to minimize inductive coupling. For typical wire inductance and Hall thruster discharge characteristics, estimates of inductive coupling in the unshielded thruster discharge lines could induce >60V peak-to-peak voltage oscillations. The conduit was grounded at each end, and extended to the thrust stand within the chamber. Electrical wiring was in twisted pairs, when possible. Thrust stand wiring and thruster electromagnets had dedicated conduit separate from thruster discharge lines. The thruster body and thrust stand shroud were electrically connected to chamber ground.

Prior to experimental measurements, the Hall thruster was run for approximately 3 hours after the initial chamber pump down to allow the system to outgas and reach thermal equilibrium. Subsequent thruster warm-up firings were conducted for 1 hour prior to experimental measurements.

B. Vacuum Facility

Experiments were conducted in the Space Environmental Facility (SPEF) at AFRL, Edwards Air Force Base. SPEF is a stainless steel, spherical vacuum chamber 9.1-m in diameter and utilizes six 48" diffusion pumps with liquid nitrogen cooled cold traps, which have demonstrated enhanced pumping capability of xenon gas. The facility has demonstrated xenon pumping speeds greater than 300,000 l/s and base pressure less than $1x10^{-6}$ torr-xenon. Two MKS Instruments cold cathode gauges (CCG) were located on the walls as shown in Fig. 3. During H6 Hall thruster operation at 10 mg/s and 20 mg/s anode flow, the operating pressure was $2.8x10^{-6}$ torr-Xe and $5.0x10^{-6}$ torr-Xe, respectively. A graphite beam dump measuring 4-meters high and 5-meters wide was positioned approximately 5 meters downstream of the thruster, shown in Fig. 3. This structure was grounded to the vacuum facility during H6 Hall thruster operation.

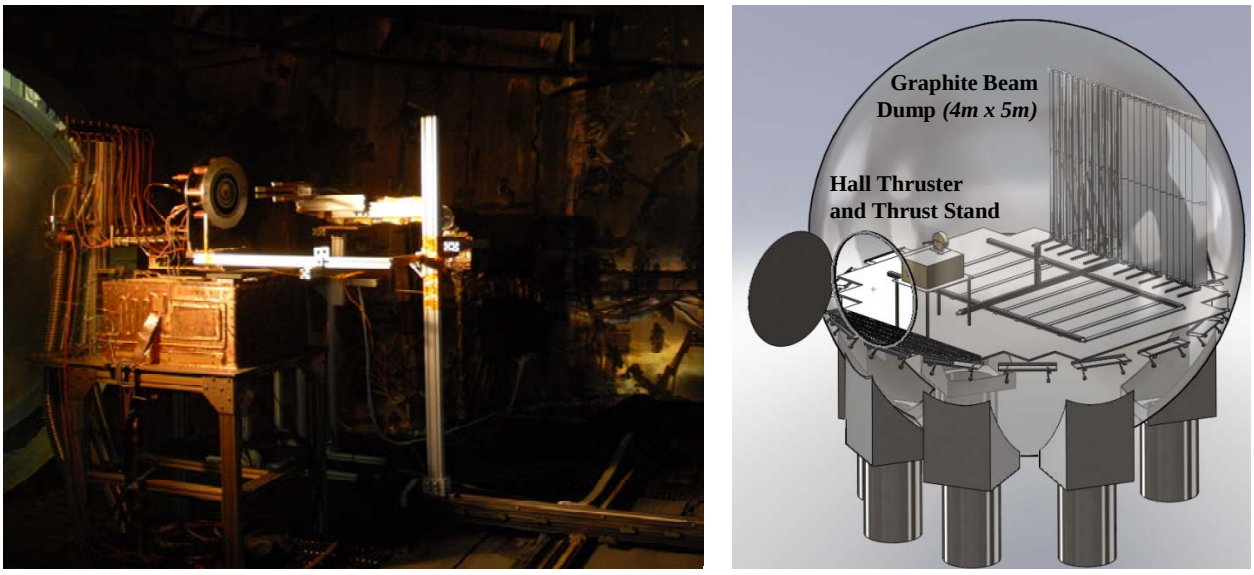

Figure 3. Experimental configuration. Left: H6 Hall thruster mounted to thrust stand in SPEF, shown with near-field probe array (not reported). Right: Solid model of SPEF vacuum chamber.

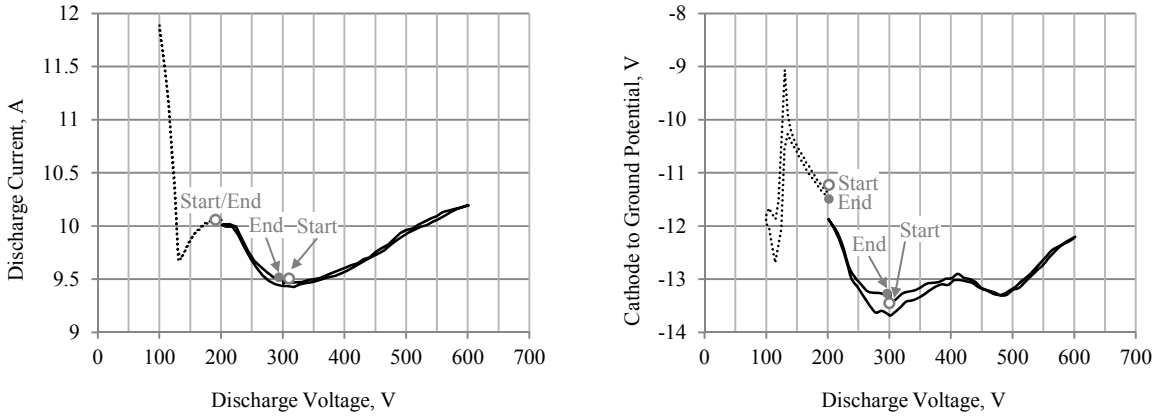

(a) **(b)**

Figure 4. H6 discharge current and cathode to ground potential for voltage sweep from (a) 100V to 200V and from (b) 200V to 600V at 10mg/s anode flow and 7% CFF.

C. Thermocouples

Thruster and cathode temperatures were monitored with Type K thermocouples. Four thermocouples (TCs) were monitored during the testing located at different locations, including TC1 at the thruster backplate near the outer electromagnet, TC2 at the backside of the front outer pole, TC3 at the LaB6 cathode mount, and TC4 at the BHC-5000 cathode mount. Thermocouple data was recorded at 0.5Hz throughout the investigation, and temperatures did not vary by more than 2°C during a voltage sweep. Although the thermocouple systematic uncertainty is 2.2°C or 0.75% of reading, the error associated with mounting is expected to be larger. Mounting error is suspected for TC3, leading to poor thermal contact which increases uncertainty in absolute temperature and temporal sensitivity to changes in surface temperature. In this investigation, thermocouple measurements were intended to assess significant variation in temperature during a sweep in discharge voltage, rather than quantify absolute temperature differences between thermocouples.

D. Data Acquisition

Characterization of the H6 operational behavior utilized a National Instruments Compact FieldPoint system, which monitored thruster discharge telemetry at the thrust stand waterfall, propellant flow from mass flow controllers, thermocouples, and background pressure. During measurement scan, discharge voltage was swept from 200V to 100V to 200V in 5V increments, with a 2 second hold at each voltage. Parameters measured at 100Hz were averaged over the final 1 second at each voltage condition. Automated measurements and data acquisition were conducted with LabView. Thruster discharge current and electromagnet currents were monitored with high accuracy current shunts. While the systematic measurement error in discharge telemetry is ±0.5%, the transient nature of these experiments increases uncertainty. This is associated with hysteresis in thruster operation, as shown in Fig. 4 for measurements of discharge current and cathode to ground potential with variation in voltage from 100V to 600V. Hysteresis in discharge current was minimal and showed consistent profiles independent of sweep direction. In addition, sweeps on separate days show difference in time-average discharge current within 2%. Hysteresis was larger in cathode to ground potential, with the difference exceeding 1V depending on sweep direction. Although this difference in cathode to ground potential reduced as the thruster operation stabilized, it indicates increased uncertainty in transient measurements. The minimal change in measured thruster and cathode temperature during a voltage sweep indicate hysteresis may be plasma phenomenon rather than a thermal effect. While hysteresis cannot be easily quantified, uncertainty in measured time-averaged discharge current and cathode to ground potential due to hysteresis is estimated at ±5% and ±20%, respectively. Hysteresis effects related to thruster mode transition will be discussed in Section V.

IV. Experimental Results

Past investigations of low-voltage H6 thruster behavior and mode transitions included detailed characterization of performance, far-field plume properties, and oscillations. Thruster behaviors were sensitive to multiple operational parameters and demonstrated hysteresis between modes, including discharge voltage, anode and cathode mass flow, cathode location, and magnetic field. To attain a better understanding of these trends, the current

Table 1. Summary of H6 test conditions, cathode configuration, and operational range

Anode Flow Rate (mg/s)	Cathode Flow Fraction (% Anode)	Discharge Voltage (V)	Electromagnet Current (A)	Electromagnet Current (A)	LaB6 Cathode (Center-mount)	BHC-5000 (External)
10	7	100-200	1.0-5.0	Inner = Outer	Yes	Yes
10	16	100-200	1.0-5.0	Inner = Outer	Yes	Yes
10*	7	100-200	1.0-5.0	Inner/Outer = 1.2	Yes	No
10*	7	100-200	1.0-5.0	Outer/Inner = 1.2	Yes	No
20	7	100-200	1.0-5.0	Inner = Outer	Yes	No
20	12	100-200	1.0-5.0	Inner = Outer	Yes	No

* Data included in Appendix.

experiments aimed to map global thruster behavior over the full operational range from 100 to 200V anode potential, and compare directly to past evaluations of changes that occur during a mode transitions. This motivation led to the test matrix in Table 1, where inner and outer electromagnet current (fixed 1:1 ratio) ranging from 1.0A to 5.0A corresponds to a maximum magnetic field on channel centerline of 45 G to 220 G, respectively. The trim coil was not used in this investigation. Evaluation of two other electromagnet ratios were assessed for10/mg/s operation with the center-mount cathode, as listed in Table 1. This data is included in the Appendix. The LaB6 cathode and BHC-5000 cathode were installed throughout testing, and switching between cathode configurations was achieved external to the chamber.

A representative voltage sweep from 200V to 100V and the return to 200V over approximately 84 seconds is shown in Fig. 5, including measured discharge current, temperatures, and cathode to ground potential. In this

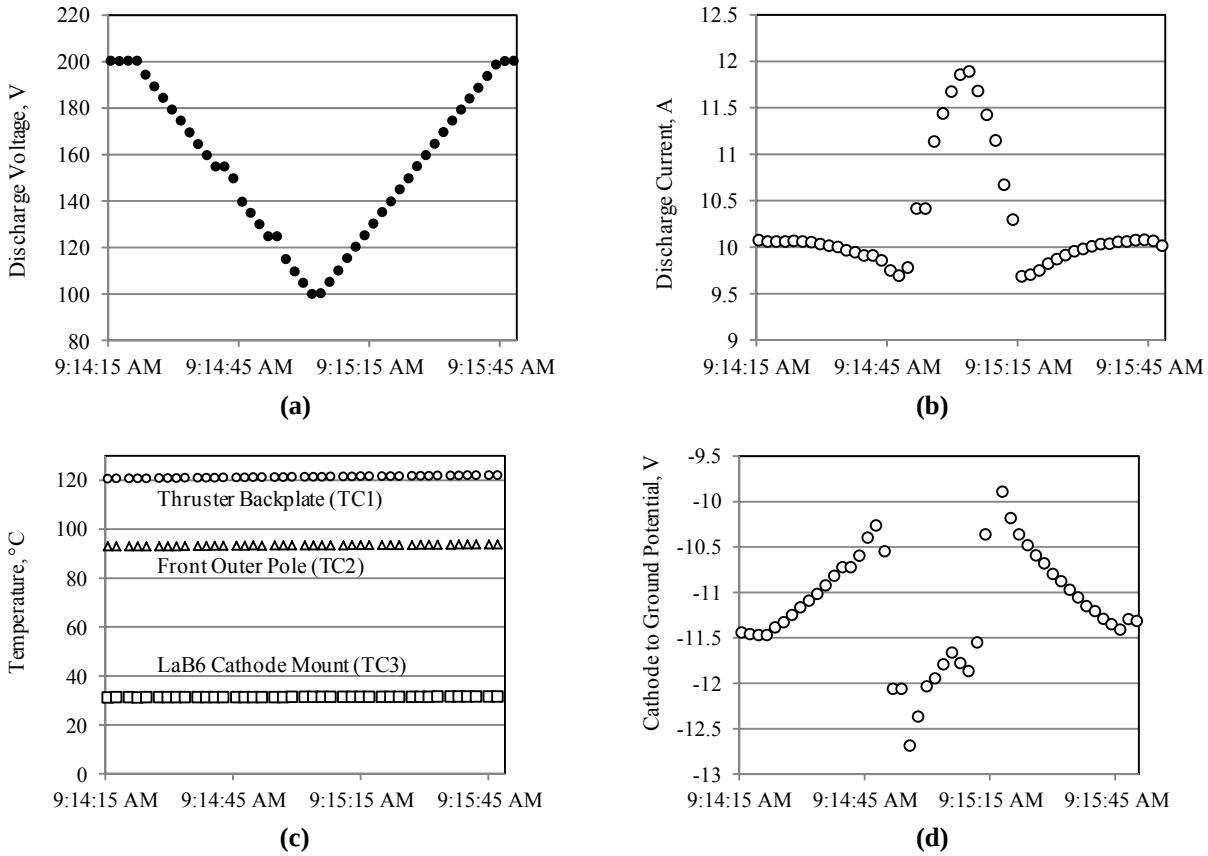

Figure 5. Discharge voltage and measured thruster parameters during voltage sweep at 10mg/s anode flow, 7% CFF with the center-mount cathode, and 2.94A on the inner and outer electromagnets, including (a) discharge voltage, (b) discharge current, (c) temperatures, and (d) cathode to ground potential.

example, the automated voltage sweep causes a change in thruster operating mode at approximately 130V discharge, as evidenced by the sharp change in discharge current >0.5A over a 2V step and change in cathode to ground potential greater than 1V. The mode associated with increased discharge current, previously designated the high-current mode or "global" mode, has demonstrated significant breathing mode oscillations and a lack of azimuthal spoke behavior.[6,10] Mode transition for this 10 mg/s operating condition occurred at approximately 130 V over a wide range of magnetic field over the course of I-V-B mapping over a 40 minute span. Although there is minimal hysteresis in discharge current in Fig. 4b, there are differences in cathode to ground potential in Fig. 4c depending on sweeping up or down in voltage. The hysteresis phenomena will be analyzed in Section IV.A.

Thermocouple data indicates thruster heating occurs over timescales greater than the voltage sweep. Over the 40 minute I-V-B characterization of this operating condition, TC1, TC2, and TC4 showed temperature increased by approximately 30°C. However, TC3 showed a lower temperature and smaller increase the 40 minute characterization of only 8°C. Despite the suspicions of poor thermal contact for TC3, trends for all thermocouples were consistent over a voltage scan and the I-V-B characterization, and therefore thermal effects are not considered a primary driver of the thruster behavior in this investigation.

A. Discharge Voltage and Magnetic Field Characterization

Discharge current is characterized as a function of discharge voltage and magnetic field for the 10 mg/s, 7% CFF operating condition with the center-mount cathode configuration is shown in Fig. 6. The mode transition at approximately 130V in Fig. 5 is evident in Fig. 6 for inner and outer electromagnet current ranging from 2.94A to 4.94A. This corresponds to a maximum magnetic field on channel centerline of 144G to 221G, respectively. The thruster exhibited less than 1A variation in time-average discharge current for anode voltage greater than 130V at magnetic field greater than 100G. Higher magnetic field resulted in higher discharge current in this regime. A transition region occurred between nominal operation in the low-current mode to the high-current mode 130V and 110V. Across this transition, discharge current increased by approximately 1A to 2A, equivalent to 10% to 20% of the discharge current. Magnetic field from 100G to 140G exhibited the largest increase in discharge current in the transition from local mode at approximately 120-130V to global mode at 110V. Below 110V, the thruster is highly oscillatory with large peak to peak current amplitude. As magnetic field is reduced to less than 100G, discharge current increases dramatically and the thruster is in a high-current mode of operation at discharge voltage approaching 200V. Below approximately 70G, the global mode was observed over the full voltage range. These oscillations intensified as magnetic field was reduced, which is consistent with past low-voltage investigations of the H6. The minimal hysteresis in measured discharge current across the full voltage sweep is consistent with Fig. 4.

The cathode to ground potential (V_{cg}) variation during the anode voltage shown in Fig. 7 corresponds to discharge current in Fig. 6 for the centrally-mounted cathode configuration. Similar characteristics are observed between discharge current and V_{cg} in the local mode, with minimal variation with voltage or magnetic field >140V and >100G. In this regime, changes in magnetic field from 100G to 221G increased the magnitude of V_{cg} by <2V. Likewise, increasing anode voltage from 140V to 200V also increased the magnitude of cathode to ground potential by <2V. There were also significant variations in the transition region between 110V to 130V, where the cathode to ground potential first increased closer to facility ground and then declined by 2V to 4V relative to the value at 140V. The increase in V_{cg} closer to facility ground is a unique feature and a key difference with the profiles of discharge current. As voltage was reduced during a sweep, this was consistently a leading indicator of the transition to global mode. It may be significant that this feature in cathode to ground potential corresponds to the lowest discharge current in the local mode for a fixed magnetic field. Another key difference between profiles of discharge current and cathode to ground potential is the hysteresis. Hysteresis in cathode to ground potential during operation in the global mode is evident in Fig. 7, and largest in the transition region. This is in contrast to discharge current, where the hysteresis is minimal and mode transition appears independent of the voltage sweep direction. This is further evidence that the cathode to ground potential is more sensitive to mode transition. The nature of the hysteresis and the behavior near the mode transition region will be discussed in Section IV. Once in the global mode, reductions in magnetic field corresponded to cathode to ground potential closer to chamber ground.

For this centrally-mounted cathode configuration, increasing from 7% CFF to 16% CFF in Figs. 8 and 9 changed conditions where the transitions occurred, however key features of the discharge current and V_{cg} remain. The transition region shifted from approximately 130V at 7% CFF to 120V at 16% CFF. In addition, the magnitude of changes in discharge current and cathode to ground potential were less for the 16% CFF condition. The cathode to ground potential was still a leading indicator of the transition and exhibited hysteresis. A new feature was observed near 200V and >150G, where the discharge current increased at higher magnetic fields and V_{cg} decreased with respect to chamber ground. As would be expected for increased total propellant flow, the discharge current increased compared to 7% CFF. At 200V operation, this increase was approximately 0.5A.

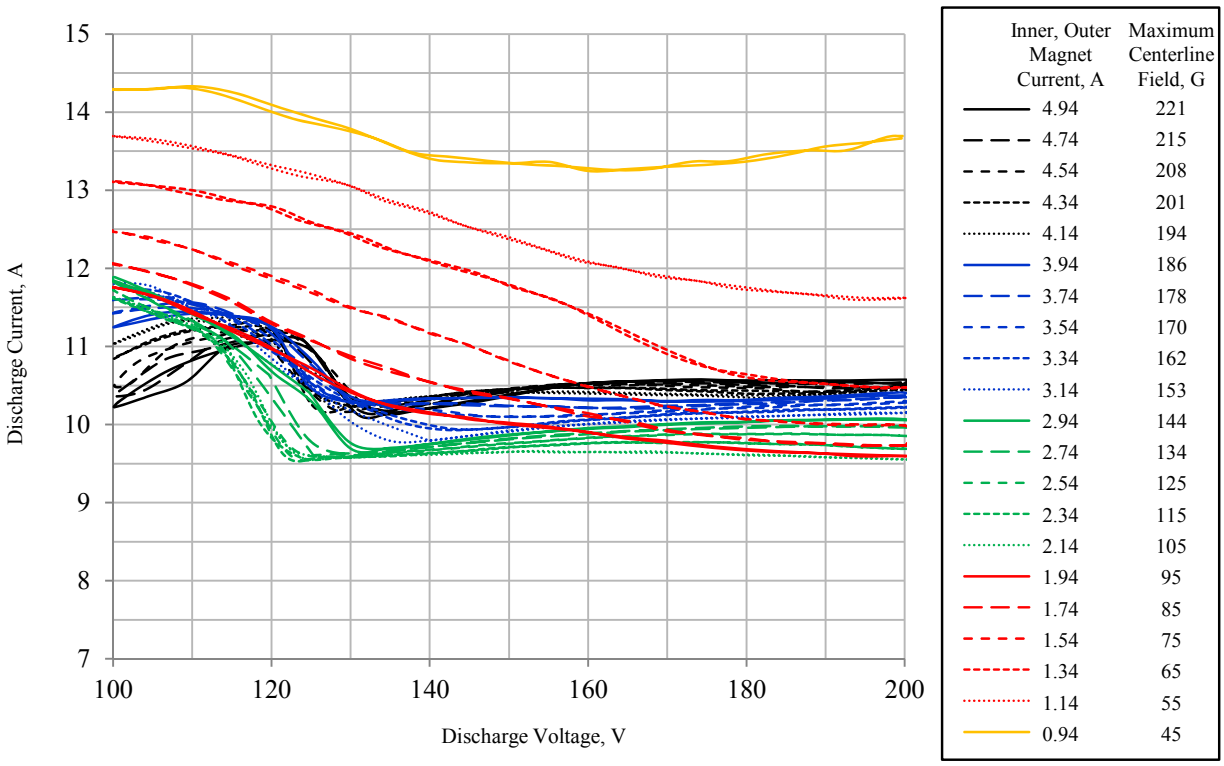

Figure 6. Discharge current as a function of discharge voltage for electromagnet current from 1.0A to 5.0A at 10mg/s anode flow and 7% CFF in the center-mount cathode configuration.

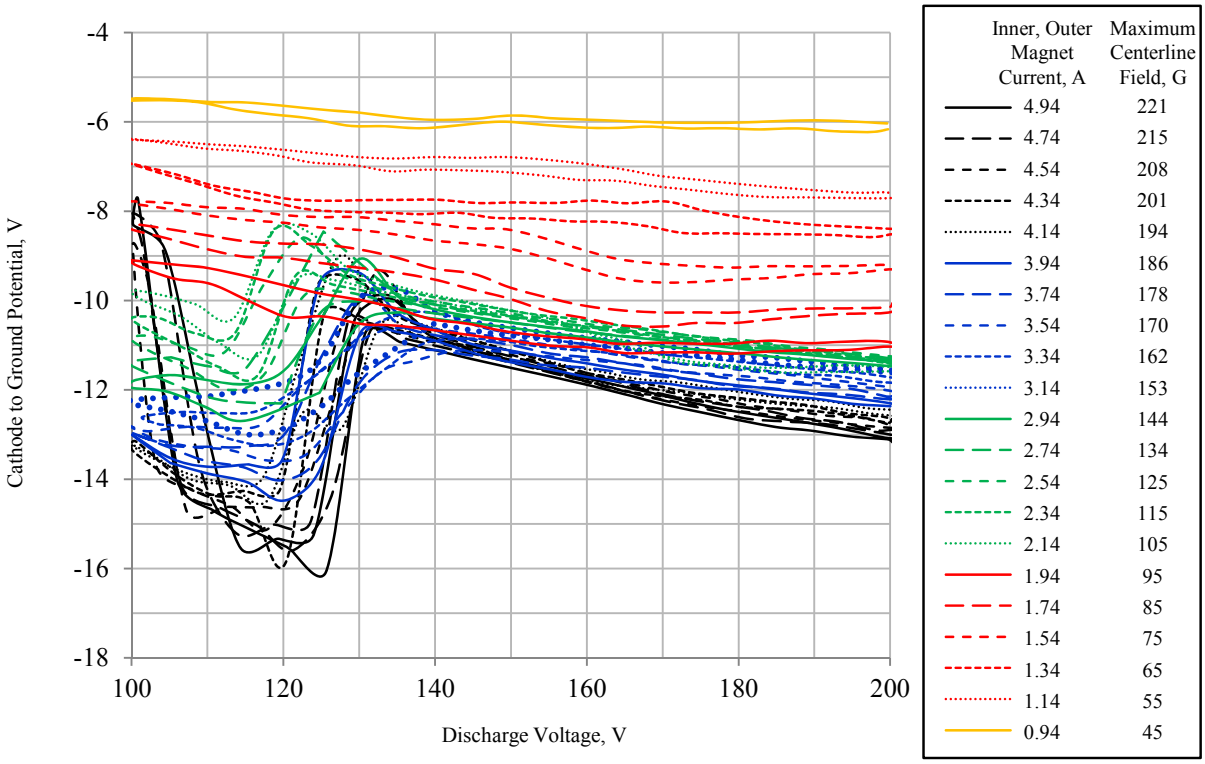

Figure 7. Cathode to ground potential as a function of discharge voltage for electromagnet current from 1.0A to 5.0A at 10mg/s anode flow and 7% CFF in the center-mount cathode configuration.

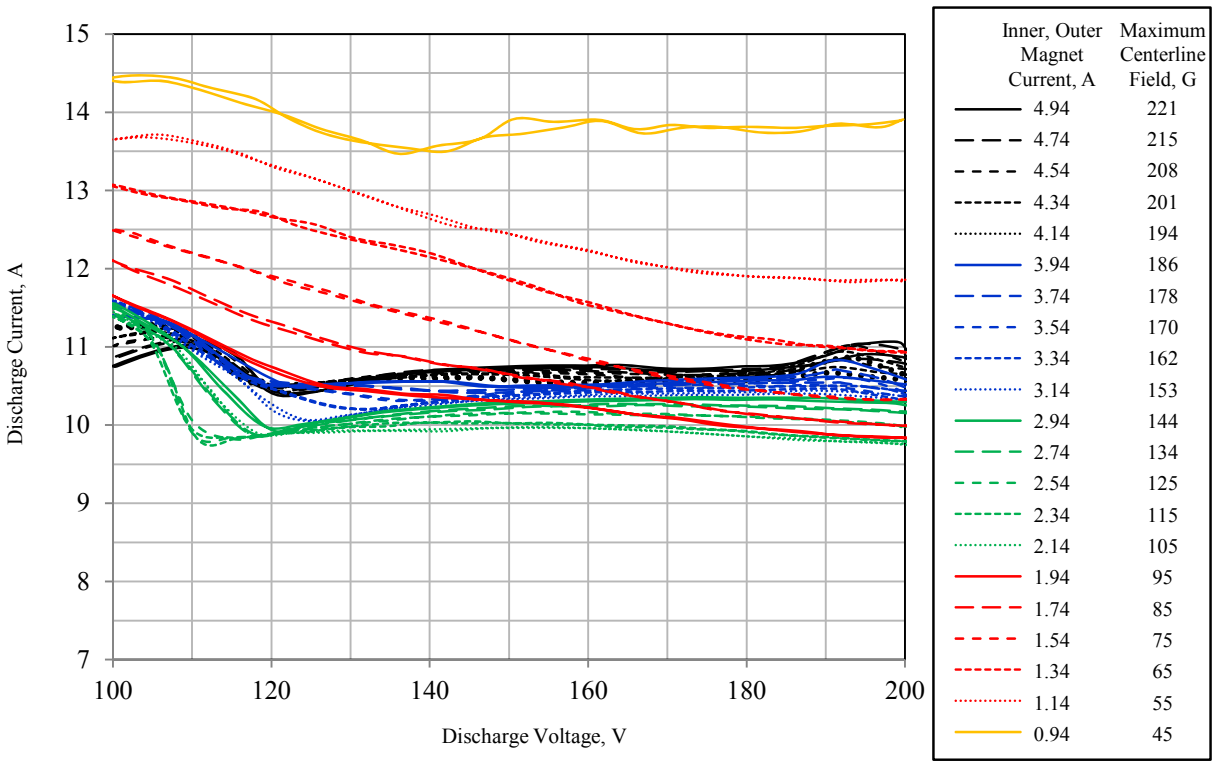

Figure 8. Discharge current as a function of discharge voltage for electromagnet current from 1.0A to 5.0A at 10mg/s anode flow and 16% CFF in the center-mount cathode configuration.

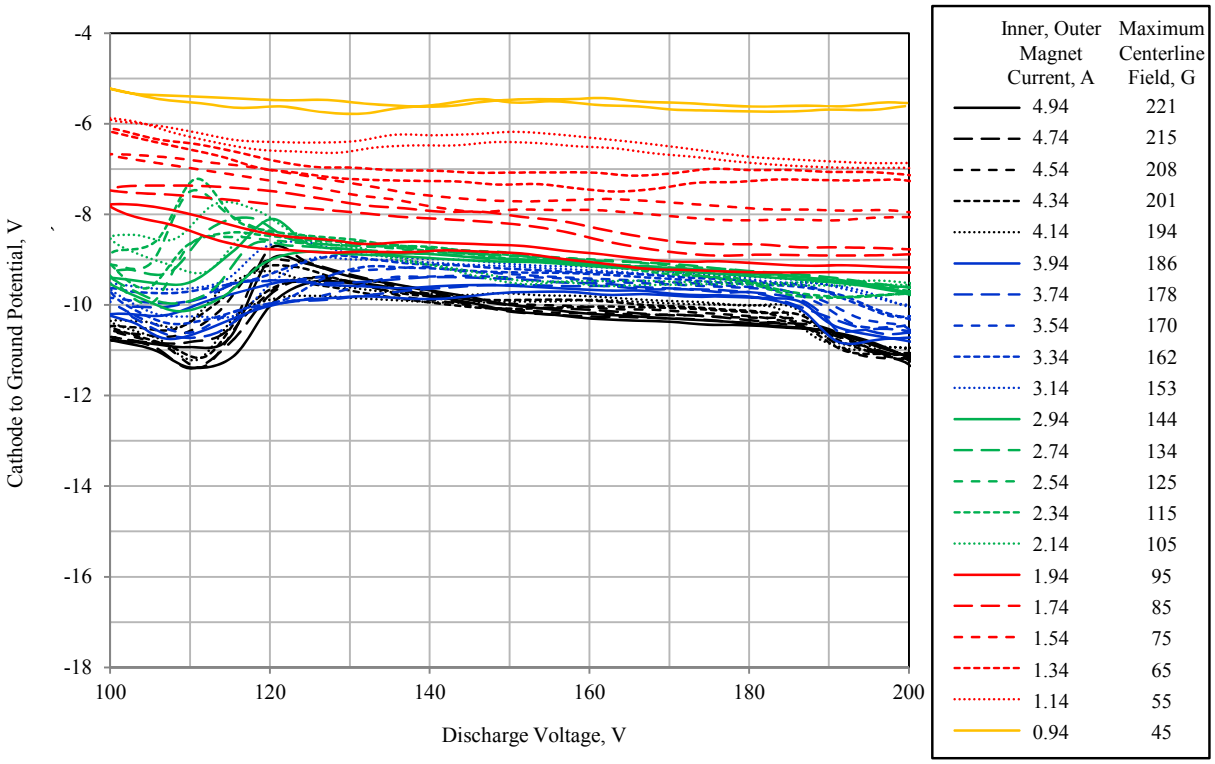

Figure 9. Cathode to ground potential as a function of discharge voltage for electromagnet current from 1.0A to 5.0A at 10mg/s anode flow and 16% CFF in the center-mount cathode configuration.

The H6 behavior with an external cathode configuration at 7% CFF is shown in Figs. 10 and 11, and exhibited significant differences with characteristics described for the center-mount cathode configuration. This characterization was conducted over the full range of magnetic field, but with fewer electromagnet settings. First, although there are features of mode transitions in the discharge current profiles, the difference in current magnitude between local and global mode in Fig. 10 are much less than that observed for the center-mount cathode configurations. For equivalent magnetic field, the transition from local to global mode occurred at a higher voltage and over a wider voltage range in the external configuration. While the time-average discharge current is consistent between the center-mount and external cathode configuration at >140V discharge and >100G, the magnitude of cathode to ground in the external configuration was 2V to 5V larger. The magnitude of cathode to ground potential in Fig. 11 showed a continuous decline at low voltage and at lower magnetic field strength, and no longer exhibited a deviation with mode transitions. Over the full discharge current profile in Fig. 10, there are no features that have a corresponding variation in the cathode to ground potential in Fig. 11. For example, the discharge current in Fig. 10 shows a sharp decline at low voltage as magnetic field is increased, with no characteristic features in cathode to ground potential in Fig. 11. This suggests that the external cathode operation is dominated by local properties or facility interactions that are independent of thruster behavior. This is further supported by the minimal hysteresis in both discharge current and cathode to ground potential during a voltage sweep. While the center-mount cathode configuration revealed hysteresis in cathode to ground potential near the mode transition, the cathode to ground potential of the external cathode configuration shows deviation <0.2V for an increasing or decreasing voltage sweep. Local magnetic field at the cathode exit is known to influence thruster cathode coupling, and may play a role in these differences. Simulations of the H6 magnetic field reveal the radial magnetic field at the cathode exit is <10G in both the center-mount and external cathode configuration.

The global thruster characteristics and differences in mode behavior associated with cathode configuration are at 10mg/s were also observed for data at 20mg/s at 7% CFF and 12% CFF in the center-mount cathode configuration and at 10mg/s at 16% CFF with the external cathode configuration. The I-V-B datasets for 10mg/s and 20mg/s conditions in Table 1 will be evaluated and discussed in Section IV.B.

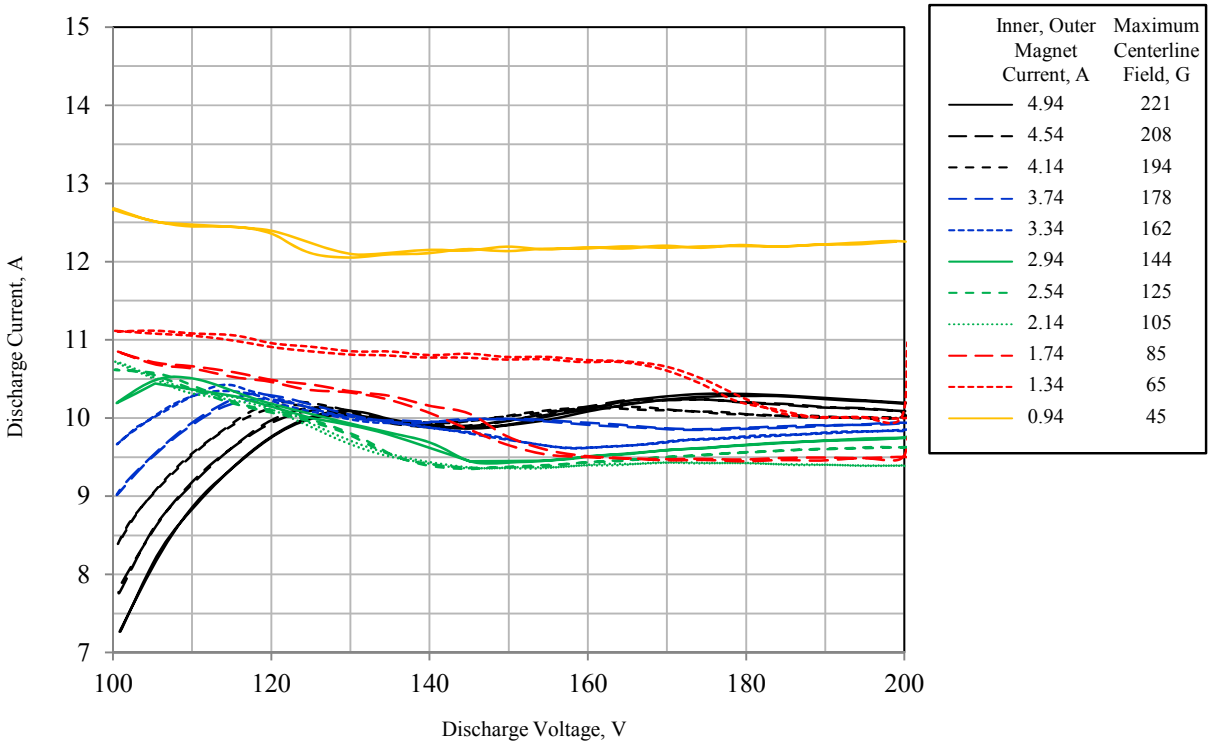

Figure 10. Discharge current as a function of discharge voltage for electromagnet current from 1A to 5A at 10mg/s anode flow and 7% CFF in the external cathode configuration.

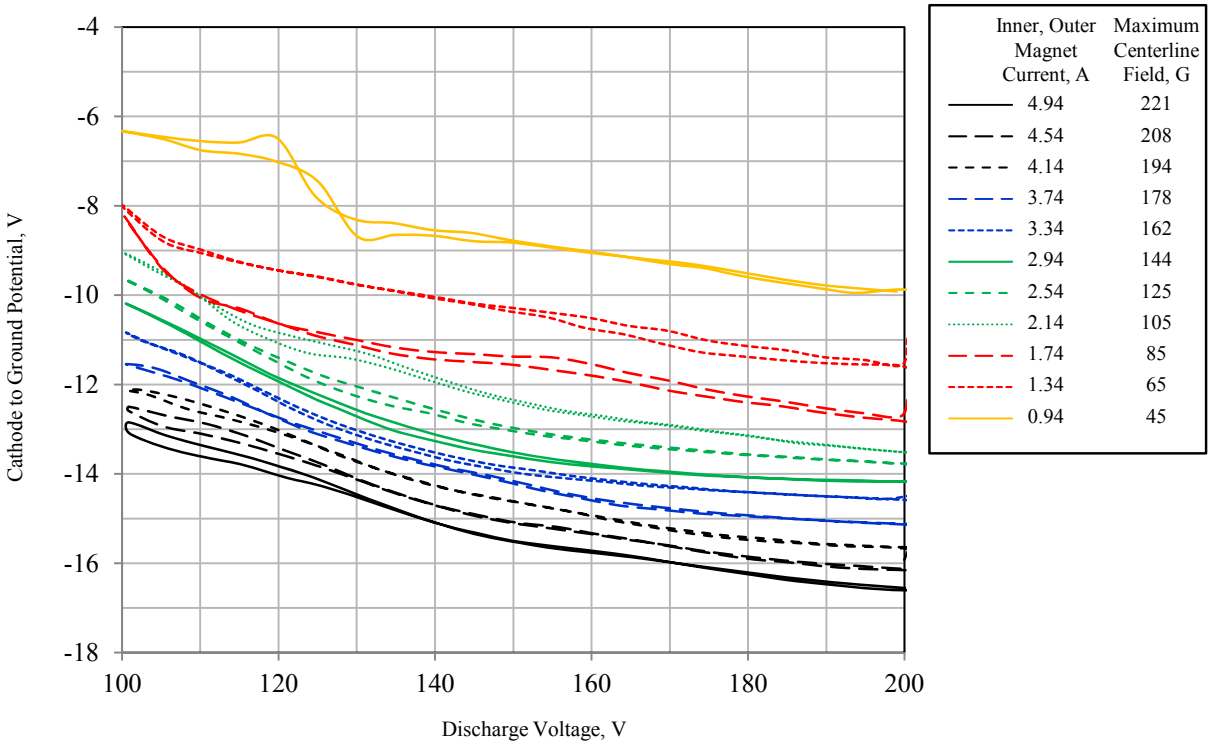

Figure 11. Cathode to ground potential as a function of discharge voltage for electromagnet current from 1A to 5A at 10mg/s anode flow and 7% CFF in the external cathode configuration.

B. Discharge Current-Voltage-Magnetic Field Mapping

Thruster I-V-B maps were developed for direct comparison of thruster characterizations in Figs. 6 through 11 and to more easily visualize regions of thruster mode behavior. Measured discharge current was averaged for a given voltage sweep and interpolated between voltage and magnetic field. A 3-dimensional I-V-B map for H6 thruster operation at 10mg/s and 7% CFF in the center-mount cathode configuration is shown in Fig. 12 from 200V to 600V and in Fig. 13 from 100V to 600V. The approach shows minimal variation in thruster discharge current over a wide range of electromagnet conditions for anode potential from 200V to 600V. This characterization shows a "valley" in Fig. 12 of minimum discharge current that occurs at increasing magnetic field for increasing voltage, which is consistent with performance characterization as a function of discharge voltage and power for typical of Hall thruster systems. In Fig. 13, the magnitude of discharge current increase during global mode operation at low-voltage is large and indicates it is a deviation from nominal thruster behavior observed at higher discharge voltage. The I-V-B mapping at 100V to 200V in Fig. 13 was taken on a separate day from the characterization at 200V to 600V, and the agreement at 200 V supports the repeatability of I-V-B maps and the notion that thermal variation during the I-V-B scans has a negligible role in these experiments.

Maps of low-voltage operation at 10mg/s anode flow in the center-mount cathode configuration are shown in Fig. 14 for 7% CFF and 16% CFF, corresponding to data in Figs. 6 and 8, respectively. In this view, the mode transition region where discharge current increased is represented by the dashed lines for each CFF. At 7% CFF, the thruster had a narrow range of magnetic field where local mode operation was possible at <120V. However, the 16% CFF shifted this transition region to lower voltages and enabled local mode operation at discharge voltage as low as 110V. Increased CFF had little effect on the thruster behavior >130V. For the same thruster conditions at 7% and 16% CFF, Fig. 16 shows I-V-B maps for the cathode in the external configuration, corresponding to data in Fig. 10 for 7% CFF. For discharge voltage >130V, the mode transition occurs at approximately the same operating conditions as the center-mount cathode configuration. However, the transition to global mode is less sensitive to small changes in discharge voltage or magnetic field strength. The mode transition below 130V is different between the center-mount and external cathode configuration. In addition, there is no perceptible difference in the I-V-B map

between 7% CFF and 16% CFF in the external cathode configuration. This may be a sign that the impact of cathode location dominates the influence of CFF.

Thruster operation at 20mg/s anode flow with the center-mount cathode in Fig. 16 shows similar trends to the 10mg/s anode flow conditions in Fig. 14. In this case, operation at 12% CFF enables operation in the local mode down to 100V discharge voltage. The transition from local mode to higher current occurred over a smaller variation in magnetic field during 20mg/s operation. Recent investigations of H6 transitions to local mode at 300V, 19.5mg/s anode flow, and 7% CFF in the center-mount cathode configuration occurred at approximately 2A on the inner magnet, which is consistent with results in Fig. 16 and implies trends at low magnetic field may extend to higher discharge voltage than shown here.[10] The I-V-B maps show minimum discharge current was achieved near the transition to the global mode for all conditions. In Section V, these trends will be compared to past experiments and assessed with knowledge gained in past investigations of the H6.

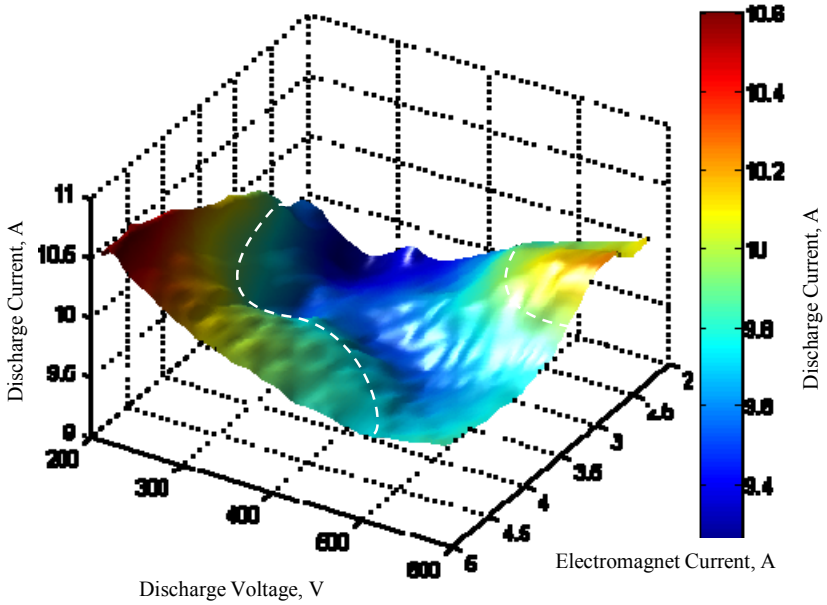

Figure 12. Discharge current as a function of discharge voltage from 100V-600V and electromagnet current from 1A-5A at 10mg/s anode flow for 7% CFF in the center-mount cathode configuration [[19]].

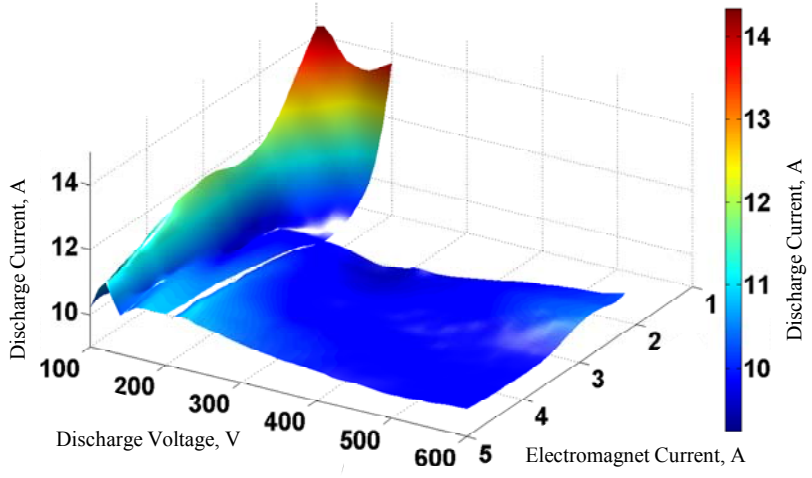

Figure 13. Discharge current as a function of discharge voltage from 200V-600V and electromagnet current from 1A-5A at 10mg/s anode flow for 7% CFF in the center-mount cathode configuration.

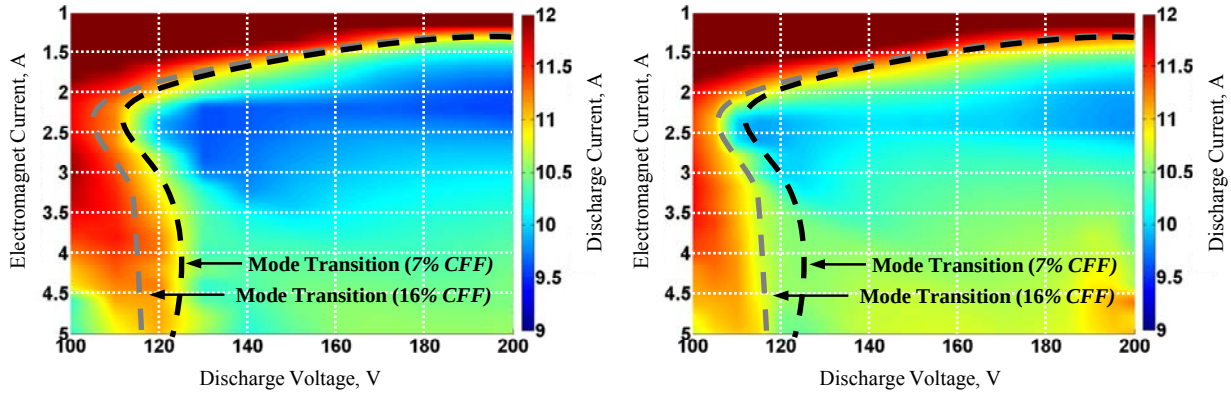

Figure 14. Discharge current as a function of discharge voltage and electromagnet current from 1A to 5A at 10mg/s anode flow for (a) 7% CFF and (b) 16% CFF in the center-mount cathode configuration. Dashed lines represent the mode transition for each CFF.

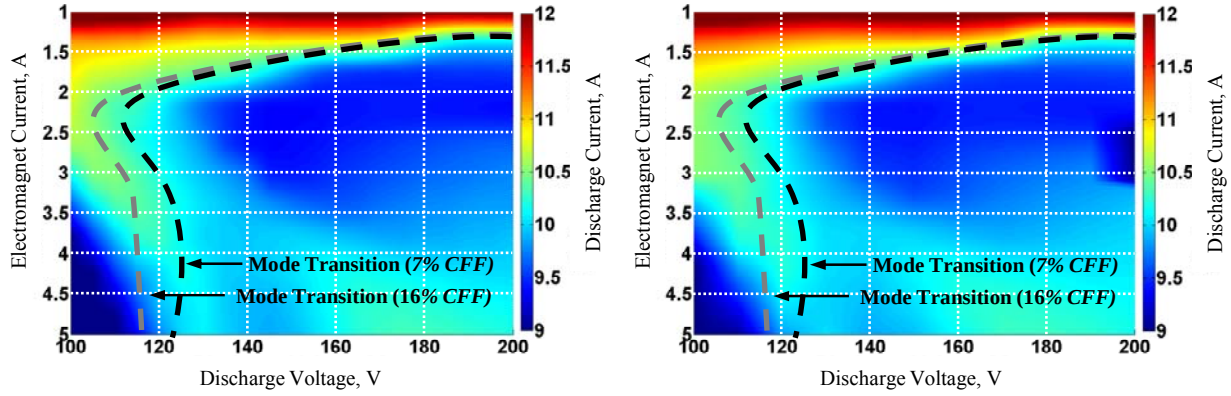

Figure 15. Discharge current as a function of discharge voltage and electromagnet current from 1A to 5A at 10mg/s anode flow for (a) 7% CFF and (b) 16% CFF in the external cathode configuration. Dashed lines represent the mode transition at 10mg/s of each CFF for the internal cathode configuration.

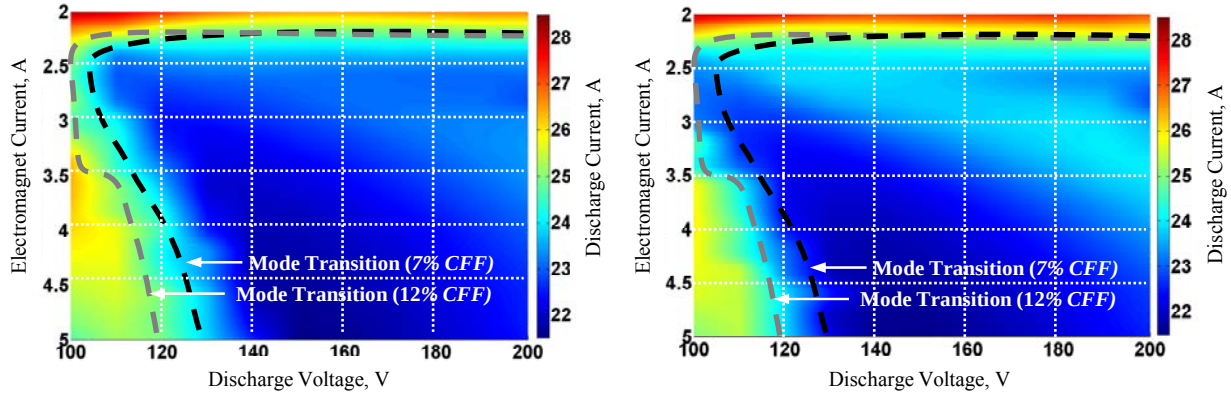

Figure 16. Discharge current as a function of discharge voltage and electromagnet current from 2A to 5A at 20mg/s anode flow for (a) 7% CFF and (b) 12% CFF in the center-mount cathode configuration. Dashed lines represent the mode transition for each CFF.

V. Discussion

Past investigations of H6 thruster operation and mode transitions have provided numerous insights into the behavior characterized in this investigation, and are summarized in Table 2. In the H6, transitions from local mode to global mode were correlated with the presence or absence of localized plasma spokes rotating azimuthally in the ExB direction.[11] Propagating plasma disturbances attributed to the azimuthal spokes have been measured over one thruster diameters downstream of the plume and are associated with reduced electron current to the anode.[6, 9,10] In the absence of spokes, the entire thruster channel oscillates in unison, designated global mode, with strong oscillation amplitude and a center spike on the thruster centerline axis. While the thrust is relatively constant between modes, the transition may exhibit mode-hopping from one behavior to the other with varying duty cycle. In time-averaged measurements, this can appear as an intermediate discharge current between the local mode and global mode mean discharge current value. To date, the mode transition has shown sensitivity to discharge voltage, magnetic field, CFF, local neutral density due to chamber background pressure or auxiliary flow. In addition, the anode flow rate, cathode configuration, and magnetic shield topology have been shown to impact this behavior.

Table 2. Summary of H6 Operational Modes

Parameter	Local Oscillation Mode (Low-Current Mode)	Global Oscillation Mode (High-Current Mode)
Discharge Oscillations	• Local spoke perturbations rotate azimuthally in the ExB direction • Small oscillation amplitude, RMS <10% mean discharge current	• Entire channel oscillates in unison, azimuthal spokes absent or negligible. • High oscillation amplitude, RMS >10% of mean discharge current.
Discharge Current	• Mean discharge current consistent with nominal thruster operation	• Elevated discharge current, 5% to 20% higher than local oscillation mode
Plume Shape	• Collimated plume, no center spike feature on thruster centerline	• Collimated plume with center spike on thruster centerline *(center-mount or external cathode)*
Thrust	• Nominal	• Nominal
Performance	• Nominal	• Reduced performance and thrust to power ratio at higher discharge current
Plasma Properties	• Nominal	• Increased electron current to anode

The data in Fig. 14 was compared directly to past investigation of the H6 at AFRL, shown in Fig. 17. Low-voltage thruster performance data at 10 mg/s from the previous study, where magnetic field was optimized for peak efficiency, is shown in Fig. 17a as a function of CFF from 7% to 26%. In Fig. 17b, the discharge current at 7% CFF in Fig. 17a is superimposed on the I-V-B map from Fig. 14. The markers for 100V to 120V are consistent with the transition line drawn on the I-V-B map, where 100V to 110V are in global mode and 115V to 120V are in local mode. Although there were minor differences in magnetic field shape between measurements in this investigation and the past study, the inner and outer electromagnets were within 0.4A for all conditions. In Appendix A, characterization of discharge current for 10 mg/s anode flow and 7% CFF to the center-mount cathode with the ratio of inner to outer electromagnet current of 1.2 in Fig. A1 shows minimal differences from Fig. A2, where the ratio of outer to inner electromagnet current was 1.2. Thus, the transition identified in I-V-B maps appear to be more sensitive to magnetic field strength than to shape, which supports the evaluation of data from past studies superimposed on the I-V-B map in Fig. 17b.

In Fig. 17c, the discharge current at 16% CFF is superimposed on the I-V-B map from Fig. 16. This data shows that at 16% CFF, all discharge voltages except 100V were capable of operation in the local mode. Overall, this analysis improves confidence that the knowledge gained in past studies of H6 mode transitions are relevant to this investigation.

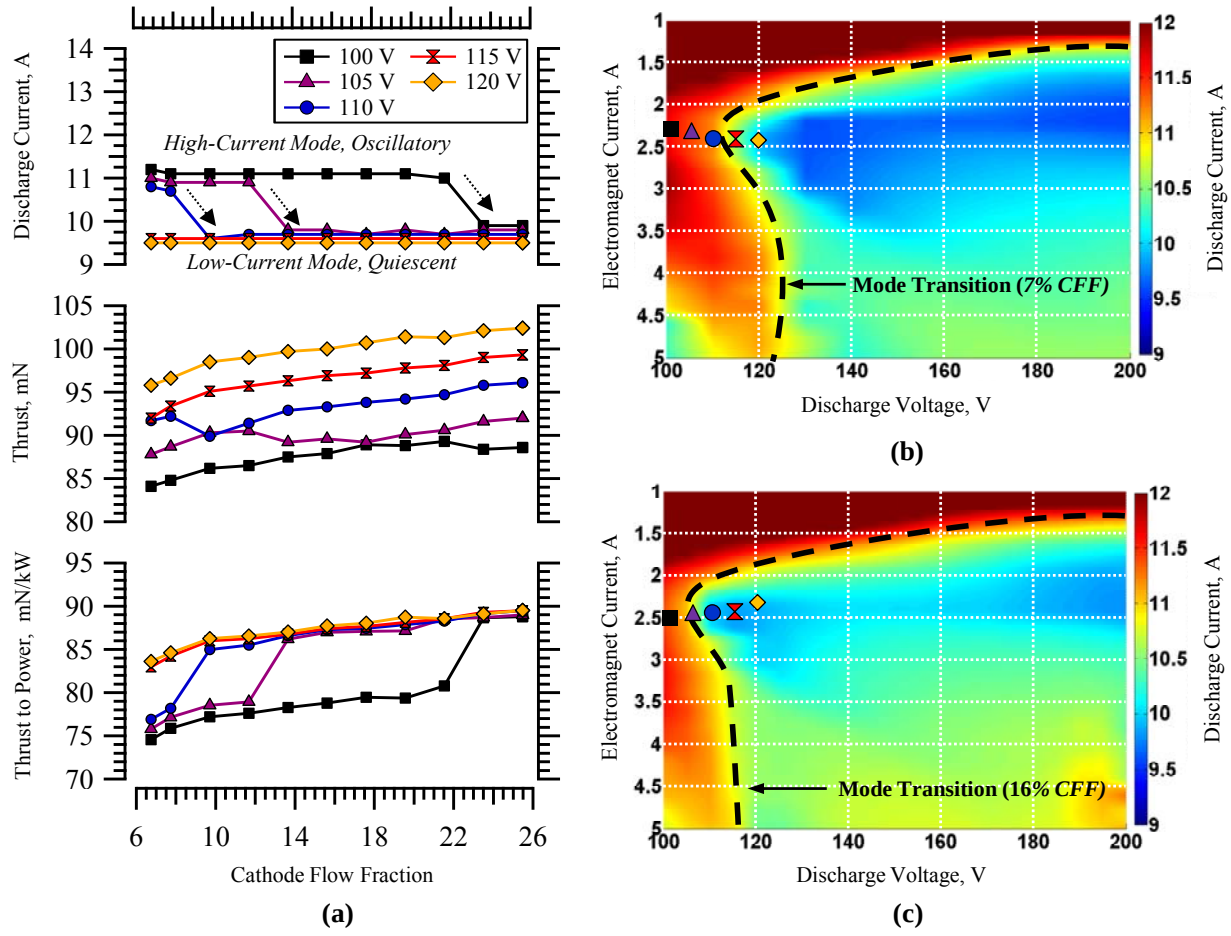

Figure 17. H6 characterization at 10mg/s anode flow for the center-mount cathode configuration as a function of (a) CFF from 7% to 26% at 100V to 120V, (b) I-V-B map from 100V to 200V at 7% CFF, and (c) I-V-B map from 100V to 200V at 16% CFF. Discharge current parameters from (a) are from a previous study and are plotted in (b) and (c).

The analysis was conducted for 20mg/s H6 operation from 100V to 120V at 7% CFF to 14% CFF in Fig. 18, with similar results. At 7% CFF, the thruster was capable of operation in the local mode at 110V to 120V, and was in global mode at 100V to 105V. Increasing CFF to 12% enabled operation in local mode at all voltages tested. The range of magnetic field where local mode was possible was larger at 20mg/s than for 10mg/s.

Far-field plume measurements of these operating modes revealed that a large fraction of the increased discharge current in global mode was due to electron current to the anode.[6] In addition, beam divergence increased. The ion energy distribution one meter downstream of channel centerline was significantly different in global mode, where the distribution was broadened and peak ion population had energy between the local mode ion energy distribution peaks for Xe^{+1} and Xe^{+2}. This indicates multiply charged ions were either created further downstream of the acceleration potential profile or underwent a charge reducing collision prior to reaching the probe location.

The nature of discharge oscillations, plasma properties, and the influence of parameters both inside and external to the discharge channel indicate the multiple plasma processes are driving the I-V-B topography. Transition regions in this investigation may be broadly categorized in two ways. First, there is a critical discharge voltage where the thruster operation transitions from local mode to global mode. Second, there is a critical magnetic field strength where the thruster transitions from local mode to global mode. The transition associated with magnetic field is relatively constant for thruster discharge voltage greater than 130 V. The magnetic field where the thruster transitions to global mode is approximately 60G to 100G. Over this range, the discharge voltage, cathode flow, and cathode configuration had minimal effect, as shown in Figs. 14, 15, and 16. This may indicate the transition is

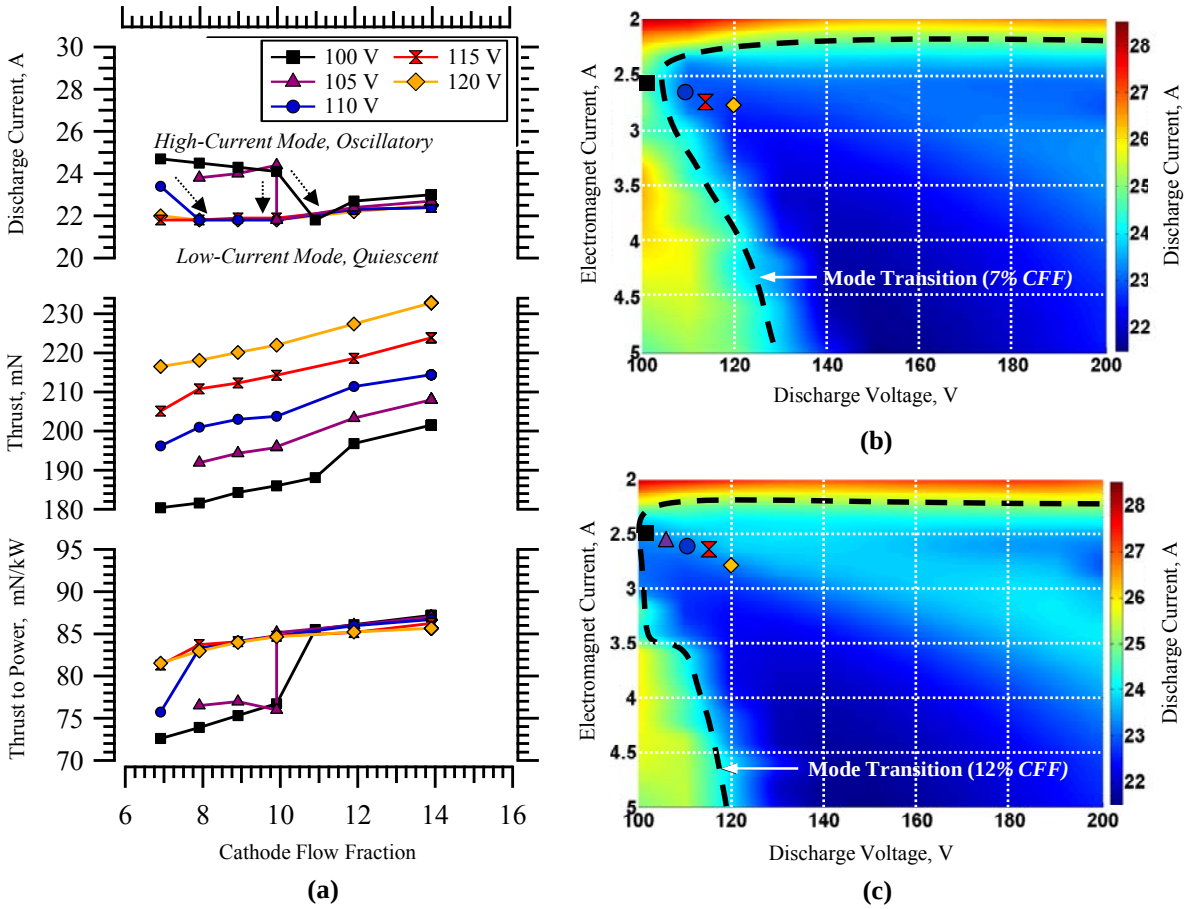

Figure 18. H6 characterization at 20mg/s anode flow for the center-mount cathode configuration as a function of (a) CFF from 7% to 14% at 100V to 120V, (b) I-V-B map from 100V to 200V at 7% CFF, and (c) I-V-B map from 100V to 200V at 12% CFF. Discharge current parameters from (a) are from a previous study and are plotted in (b) and (c).

driven by processes internal to the discharge channel, such the classical electron Hall parameter Ω_e in Eq. (1) or the cross field electron mobility $\mu_{e\perp}$ in Eq. 2.

$$\Omega_e = \frac{e\,B}{\nu_e\, m_e} \tag{1}$$

$$\mu_{e\perp} = \frac{e}{\nu_e\, m_e}\left(\frac{1}{1+\Omega_e^2}\right) \approx \frac{\nu_e\, m_e}{e\,B_r^2} \tag{2}$$

where m_e is the electron mass ($9.109\text{x}10^{-31}$ kg), e is the electron charge ($1.602\text{x}10^{-19}$ C), and υ_e is the total effective electron collision frequency, including electron-neutral collision frequency, electron-ion collision frequency, electron collision frequency with channel walls, and a collision frequency accounting for turbulent plasma fluctuations. Past studies of total effective electron collision frequency have estimated $1\text{x}10^7$ Hz for the H6 Hall thruster acceleration region at 20mg/s, which decreased to approximately $5\text{x}10^6$ Hz at 10mg/s.[13,20] In order to sustain Hall thruster operation, the electron Hall parameter must be much greater than unity.

Another parameter to be considered is the electron gyroradius, which must be much shorter than the length scale of the discharge acceleration zone. For the H6, this zone has been shown to be approximately 10mm to 20mm for based on internal plasma measurements at 150V and 300V, respectively.[13] The electron gyroradius r_e is calculated as the ratio of electron thermal velocity to electro cyclotron frequency, and may be expressed as a function of magnetic field and electron temperature T_e in Eq. (3) as:

$$r_e = \sqrt{\frac{k\,T_e}{m_e}}\,\frac{m_e}{e\,B} \tag{3}$$

where k is the Boltzmann constant (1.3807×10^{-23} J/K).

Qualitative evaluation of these parameters is presented in Figs. 19, 20, and 21, where contours of constant electron gyroradius, electron Hall parameter and cross-field electron mobility are overlaid on I-V-B maps of 10mg/s and 20mg/s operation for the center-mount cathode configuration. In this analysis, the electron temperature was approximated as 20eV for 200V discharge, and reduced linearly to 15eV at 100V discharge. Total effective electron collision frequency was estimated at 5×10^6 Hz for analysis of 10mg/s operation and 1×10^7 Hz for 20mg/s operation. The peak radial magnetic field was used for all cases.

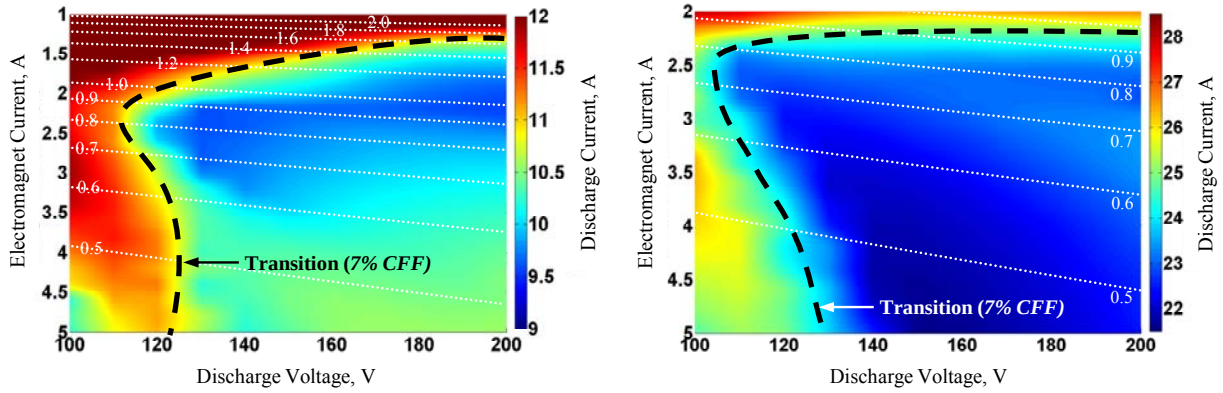

Figure 19. Discharge current as a function of discharge voltage and electromagnet current with contours of constant electron gyroradius in mm for (a) 10mg/s anode flow for 7% CFF to the center-mount cathode and (b) 20mg/s anode flow for 7% CFF to the center-mount cathode.

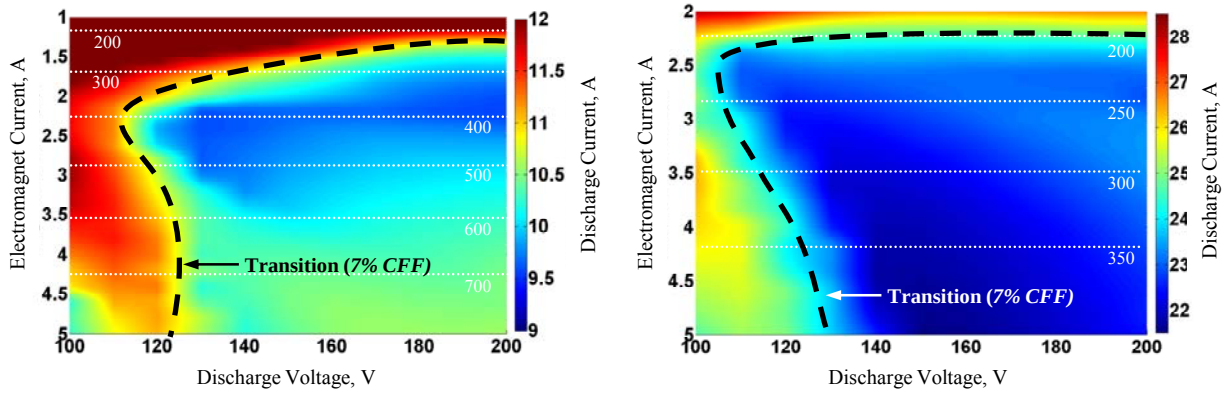

Figure 20. Discharge current as a function of discharge voltage and electromagnet current with contours of constant electron Hall parameter for (a) 10mg/s anode flow for 7% CFF to the center-mount cathode and (b) 20mg/s anode flow for 7% CFF to the center-mount cathode.

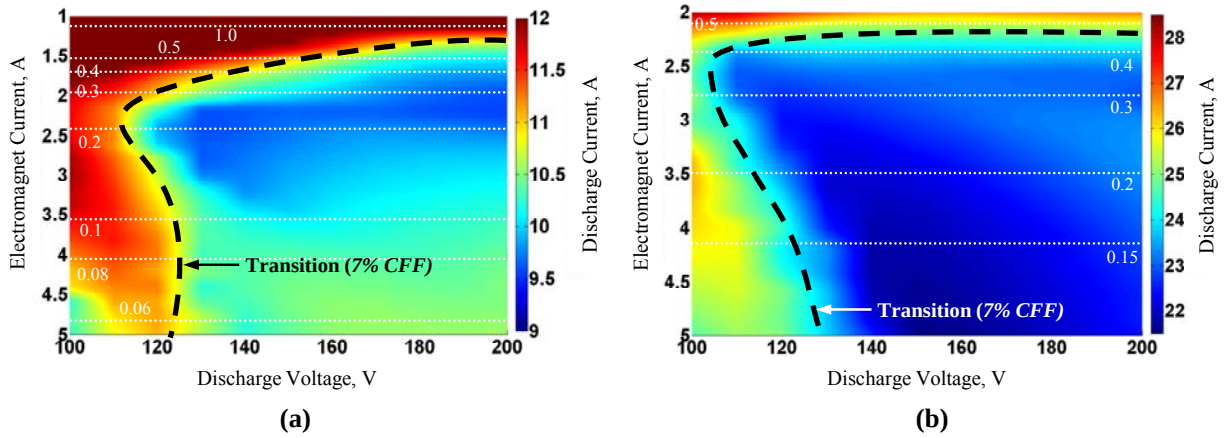

Figure 21. Discharge current as a function of discharge voltage and electromagnet current with contours of constant cross-field electron mobility in $m^2V^{-1}s^{-1}$ for (a) 10mg/s anode flow for 7% CFF to the center-mount cathode and (b) 20mg/s anode flow for 7% CFF to the center-mount cathode.

The contours of electron gyroradius <2.0mm in Fig. 19 are lower than the expected characteristic length of the thruster discharge, and do not appear to follow the trends in I-V-B maps in this analysis. While the electron Hall parameter in Fig. 20 does not show trends for the low-voltage transition <130V, there is consistency between the contour where Ωe=200 for both 10mg/s and 20mg/s anode flow conditions the transition at 200V. The Ωe=200 contour shows better agreement with the 20mg/s I-V-B map over a wide range of voltage from approximately 120V to 200V. It should be noted that past estimates of the electron Hall current in the H6 acceleration zone were also in this range for nominal operation, and within the uncertainty of this qualitative analysis.[13] Contours of constant cross-field electron transport in the near-exit region in Fig. 21 also follow the transition at low magnetic field, when $\mu_{e\perp}$ is approximately 0.4 to 1 $m^2V^{-1}s^{-1}$. The cross-field mobility increases rapidly as magnetic field strength is reduced. Both the Hall parameter and the cross-field electron transport vary significantly outside of the discharge channel, and are dynamic properties that may vary locally in space and time. Evaluation of the H6 total Hall parameter by Reid identified electron-neutral collision frequency as the dominant mechanism driving changes in the location of ionization and acceleration at different anode flow rates, where higher flows corresponded to Hall current extending outside of the discharge channel.[13] Since the mode transition with reduced magnetic field did not vary with voltage from 130V to 200V, the trends at likely associated with magnetic field and transition behavior may extend >300V.

The transition associated with reduced discharge voltage is more complex, and is shown to be influenced by cathode configuration and cathode flow fraction. This was also sensitive to neutral propellant injected near the cathode exit, thereby suggesting the near-field neutral flow is partly responsible for the mode transition behavior. The complex interactions between mode transition at <130V suggests near-field neutral density plays a strong role, along with cathode coupling and potentially facility interactions. This warrants further evaluation and consideration for Hall thrusters designed for high T/P operation.

VI. Conclusions

Investigations of low-voltage Hall thruster operation identified mode transition behavior associated with low-magnetic field strength and low anode potential. Maps of global I-V-B thruster operation revealed the location of minimum discharge current and peak T/P operation is near the transition to global mode operation, associated with high discharge current oscillations, increased electron current to the anode, and reduced efficiency. The complex nature of mode transitions and evaluation of cathode to ground potential indicates there may be facility interactions influencing the thruster operation. The I-V-B topologies and mode transitions were evaluated with respect to fundamental electron dynamics critical for Hall thruster operation, including the electron Hall parameter, electron gyroradius, and cross-field electron mobility. Mode transitions at low voltage may be related to reduced electron Hall parameter and increased cross-field electron transport. However, qualitative assessment of bulk discharge properties are limited, and assessment of time-resolved and spatially resolved plasma properties near the exit plan are recommended.

Appendix

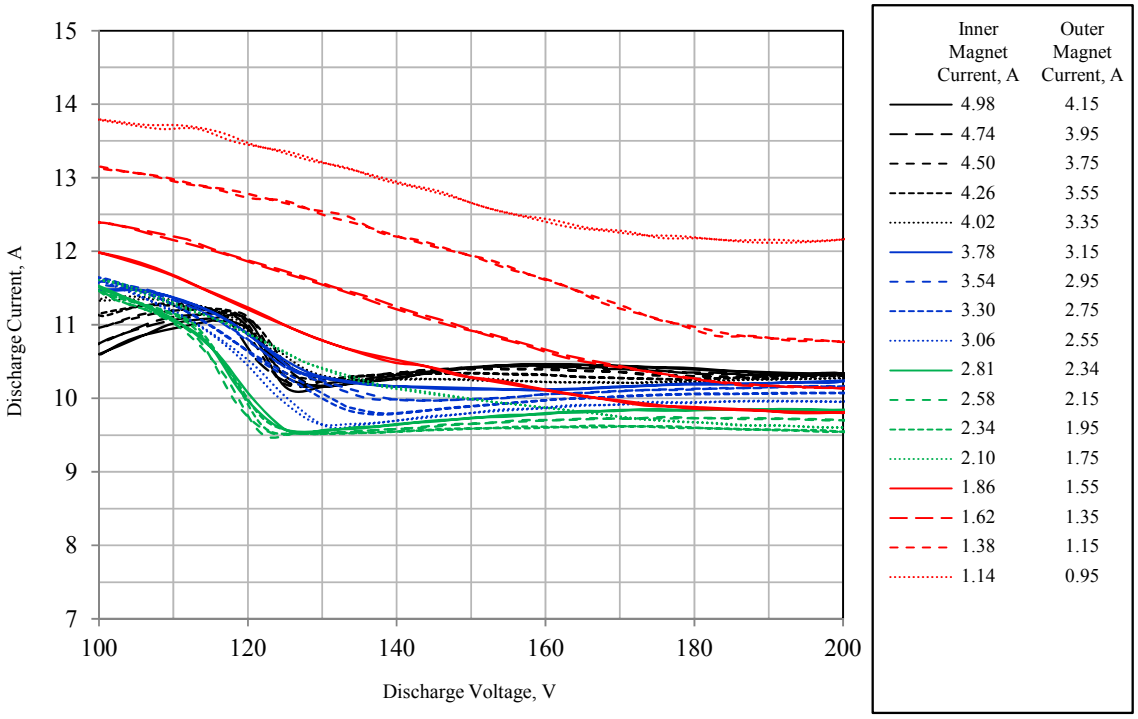

Figure A1. Discharge current as a function of discharge voltage at 10mg/s anode flow and 7% CFF in the center-mount cathode configuration, for the ratio of inner to outer electromagnet current fixed at 1.2.

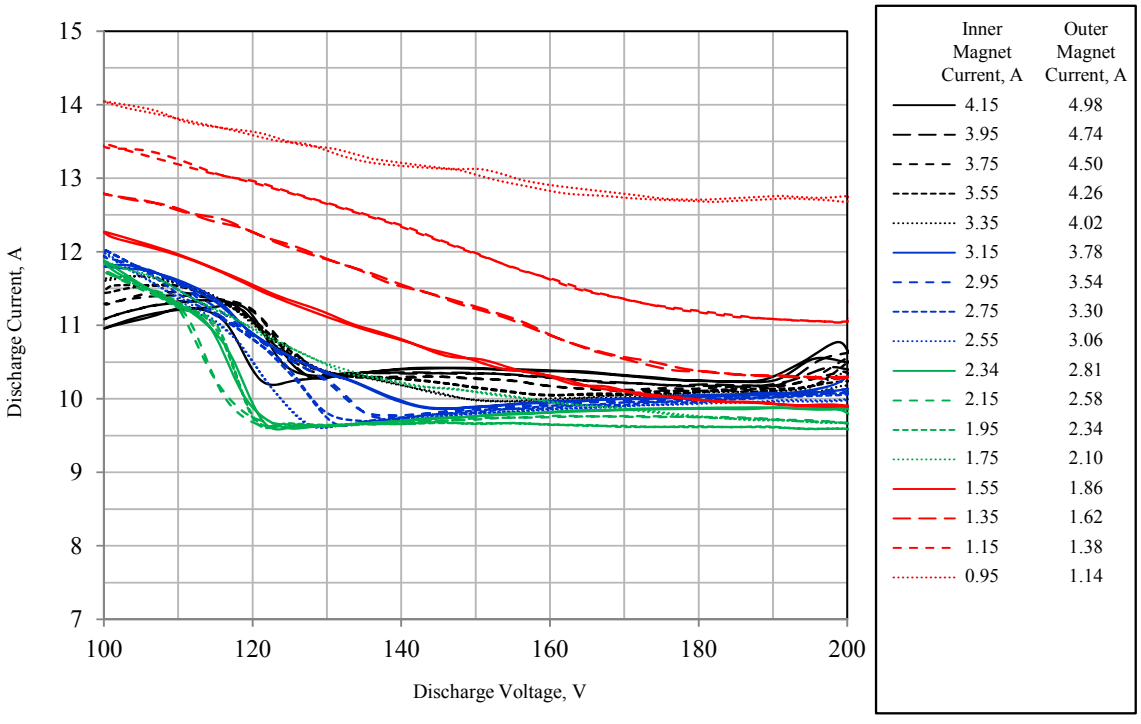

Figure A2. Discharge current as a function of discharge voltage at 10mg/s anode flow and 7% CFF in the center-mount cathode configuration, for the ratio of outer to inner electromagnet current fixed at 1.2.

References

[1] Tilinin, G., *Sov. Phys. Tech. Phys*., 22, 974, 1977.

[2] Esipchuck, Y., Morozov, A., Tilinin, G., Trofimov, A., *Sov. Phys. Tech. Phys*., Vol. 18, pp. 928, 1974.

[3] Choueiri, E. Y., "Plasma Oscillations in Hall Thrusters," *Physics of Plasmas*, Vol. 8, No. 4, April 2001.

[4] Chesta, E., Lam, C. M., Meezan, N. B., Schmidt, D. P., Cappelli, M. A., "A Characterization of Plasma Fluctuations within a Hall Discharge," *IEEE Transactions on Plasma Science*, Vol. 29, No. 4, August 2001.

[5] Azziz, Y., "Experimental and Theoretical Characterization of a Hall Thruster Plume," Doctoral Dissertation, Department of Aeronautics and Astronautics, Massachusetts Institute of Technology, Cambridge, MA, 2007.

[6] Brown, D. L., Gallimore, A. D., "Investigation of Low Discharge Voltage Hall Thruster Operating Modes and Ionization Processes," 31st International Electric Propulsion Conference, IEPC-2009-074, Ann Arbor, MI, September 20-24, 2009.

[7] Meezan, N. B., Hargus Jr., W. A., Cappelli, M. A., "Optical and Electrostatic Characterization of Oscillatory Hall Discharge Behavior," AIAA-98-3502, Cleveland, OH, July 13-15, 1998.

[8] Gascon, N., Perot, C., Bonhomme, G., Caron, X., Bechu, S., Lasgorceix, P., Izrar, B., Dudeck, M., "Signal Processing and Non-Linear Behavior of a Stationary Plasma Thruster: First Results," AIAA-99-2427, Los Angeles, CA, June 20-24, 1999.

[9] M. Sekerak, B. Longmier, A. Gallimore, D. Brown, R. Hofer and J. Polk, "Azimuthal Spoke Propagation in Hall Effect Thrusters," IEPC-2013-143, 33rd International Electric Propulsion Conference, Washington, D.C., October 6-10, 2013.

[10] Sekerak, M. J., Longmier, B. W., Gallimore, A. D., Brown, D. L., Hofer, R. R., Polk, J. E., "Mode Transitions in Hall Effect Thrusters," AIAA 2013-4116, San Jose, CA, July 14-17, 2013.

[11] McDonald, M., Gallimore, A., "Parametric Investigation of the Rotating Spoke Instability in Hall Thrusters," IEPC-2011-242, 32nd International Electric Propulsion Conference, Wiesbaden, Germany, September 11-15, 2011.

[12] D. L. Brown, "Investigation of Low Discharge Voltage Hall Thruster Characteristics and Evaluation of Loss Mechanisms," Ph.D. Dissertation, University of Michigan, Ann Arbor, MI, 2009.

[13] B. M. Reid, "The Influence of Neutral Flow Rate in the Operation of Hall Thrusters," Ph.D. Dissertation, University of Michigan, Ann Arbor, MI, 2009.

[14] K. K. Jameson, "Investigation of Hollow Cathode Effects on Total Thruster Efficeincy in a 6-kW Hall Thruster," Ph.D. Dissertation, University of California, Los Angeles, CA, 2008.

[15] J. M. Haas, F. S. Gulczinski III, A. D. Gallimore, G. G. Spanjers, and R. A. Spores, AIAA Paper No. 98-3503, 1998.

[16] R. R. Hofer, R. S. Jankovsky, and A. D. Gallimore, J. Propul. Power 22, 721 (2006).

[17] R. R. Hofer and A. D. Gallimore, J. Propul. Power 22, 732 (2006).

[18] D. M. Goebel and R. M. Watkins, Rev. Sci. Instrum. 81, 083504 (2010).

[19] Brown, D. L., "Electric Propulsion Test and Evaluation Methodologies for Plasma in the Environment of Space and Testing," Presented at the 3rd AFRL/RQR 6.1 Review, AFTC/PA Clearance No. 14013, 28-30 January, 2014.

[20] Hofer, R. R., Katz, I., Mikellides, I. G., Goebel, D. M., Jameson, K. K., Sullivan, R. M., Johnson, L. K., , "Efficacy of Electron Mobility Models in Hybrid-PIC Hall Thruster Simulations," AIAA 2008-4924, Hartford, CT, July 21-23, 2008.

Integrity ★ Service ★ Excellence

Low-Voltage Hall Thruster Mode Transitions

50th AIAA/ASME/SAE/ASEE Joint Propulsion Conference & Exhibit, AIAA-2014-XXXX, Cleveland, OH, 28 – 30 July, 2014

Daniel L. Brown[1]

Robert B. Lobbia[2]

Joseph M. Blakely[2]

Air Force Research Laboratory

Edwards AFB, CA

[1] In-Space Propulsion Branch (RQRS)

[2*] ERC, Inc

AFRL

Outline

- Background and Motivation
- Experimental Apparatus and Approach
- Results
  - Characterization of Voltage and Magnetic Field
  - Current-Voltage-Magnetic Field (I-V-B) Mapping
- Comparison to Past Investigations
- Analysis of Bulk Electron Parameters
- Summary and Conclusions

Background – 1

In 2007…

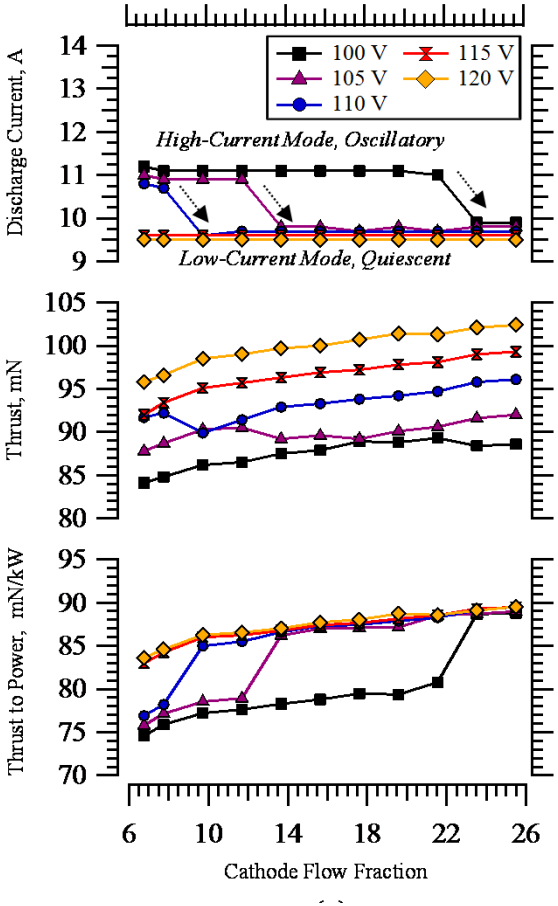

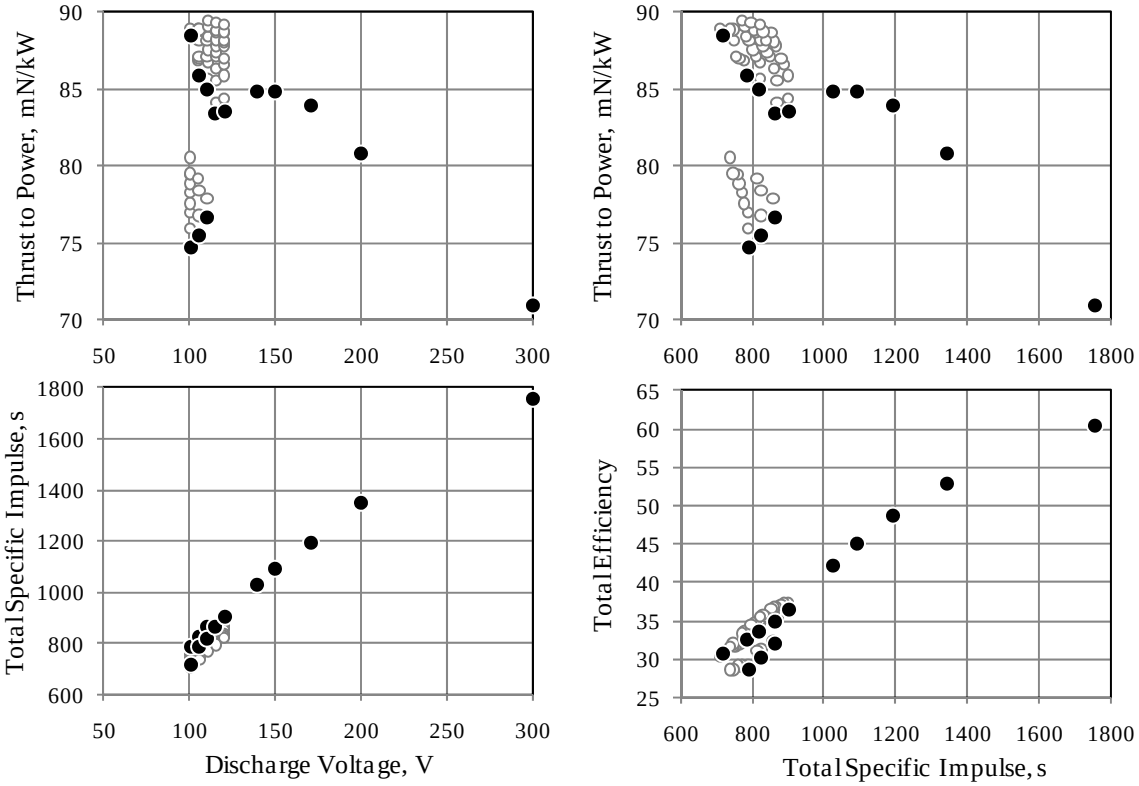

Past Investigations of High Thrust-to-Power Reveal Low-Voltage Hall Thruster Mode Transitions

- >10% change in discharge current
- Sensitive to Vd, B, CFF, near-field neutral density

Background – 2

Discharge Current Oscillations: 105 V, 20 mg/s, 10% CFF

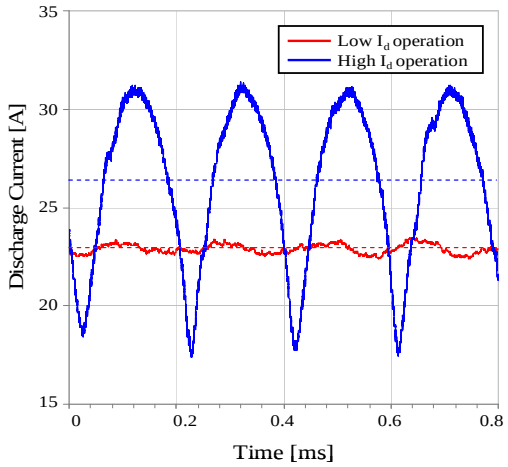

Faraday: 105 V, 10-20 mg/s, 16 CFF (1.0 m)

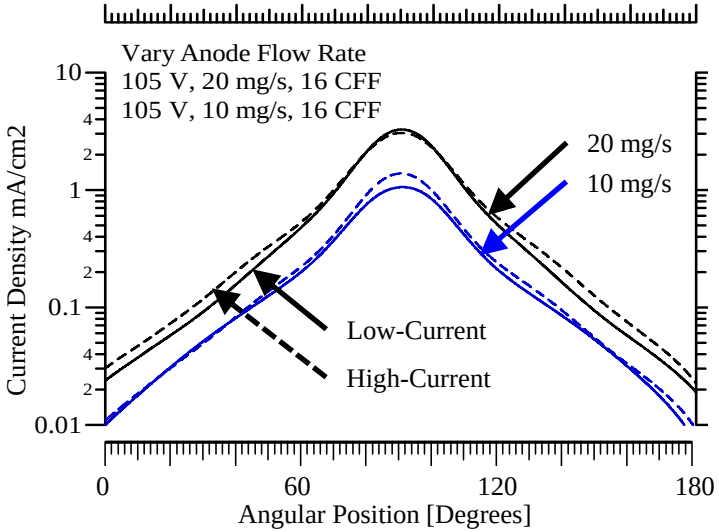

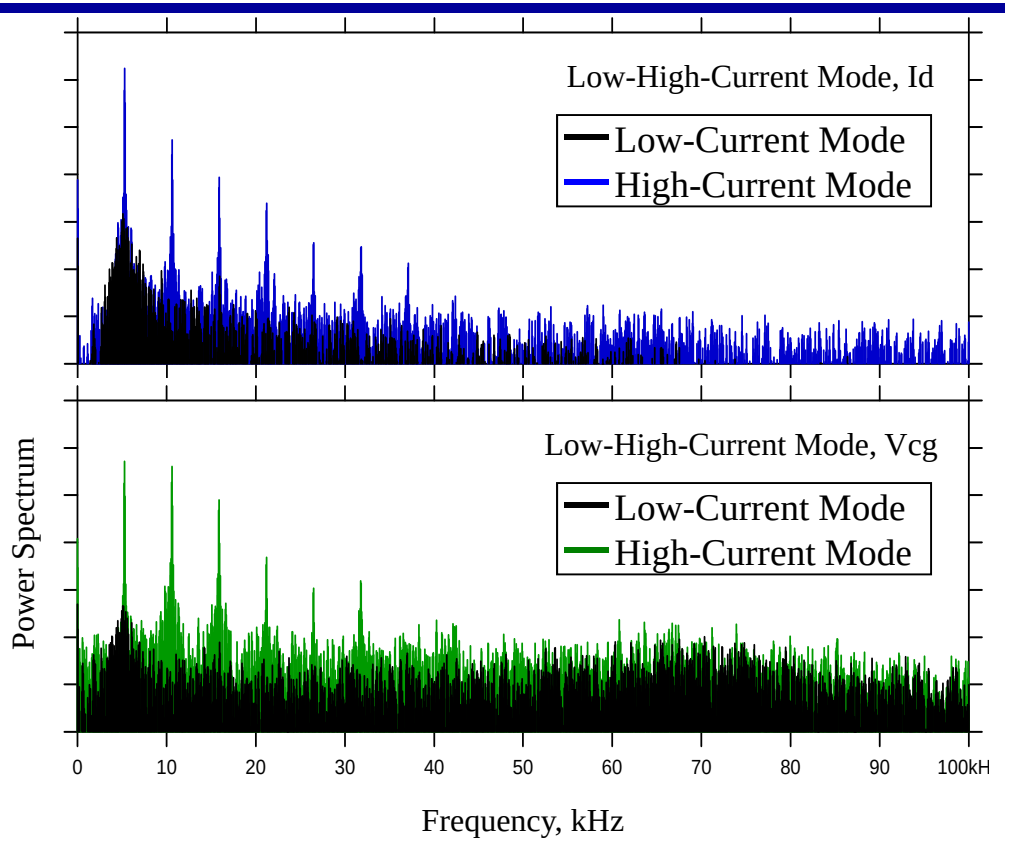

Large increase in oscillation amplitude – discharge current and cathode to ground potential

Large increase in electron current to anode

Change in Electron Dynamics and Discharge Processes

Background – 3

Ion Energy Diagnostics

- dispersion of ion energy in High-current mode
- RPA most probable ion potential is constant
- secondary ExB peak possibly due to:
  - (1) CEX collision resulting in high energy Xe^{+}
  - (2) CEX collision resulting in low energy Xe^{2+}
  - (3) Two primary ionization regions

ExB: 105 V, 20 mg/s, 10 CFF (1.0 to 1.3 m)

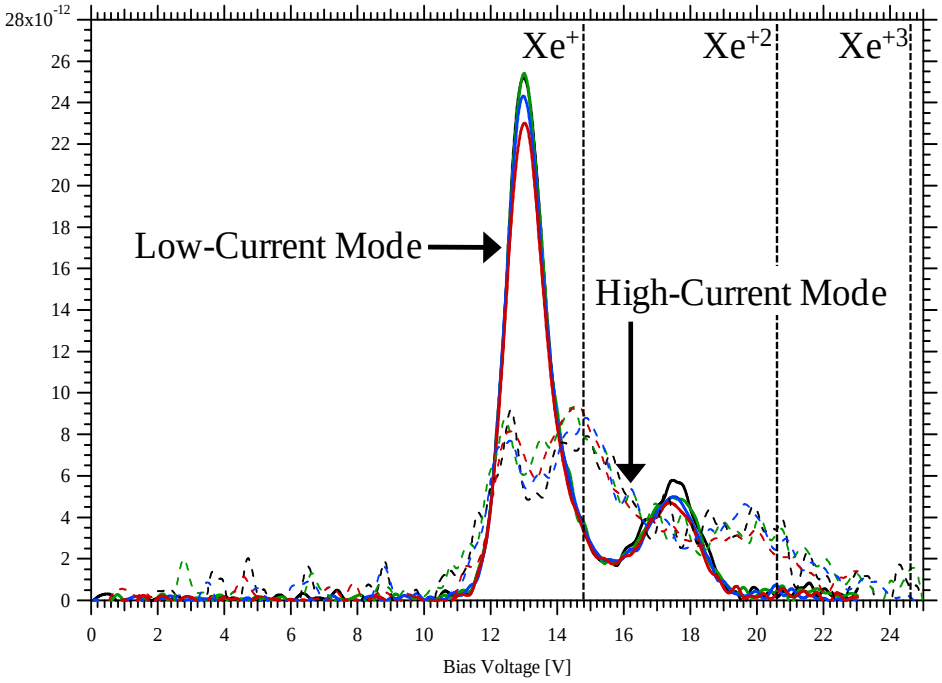

RPA: 105 V, 20 mg/s, 8-16 CFF

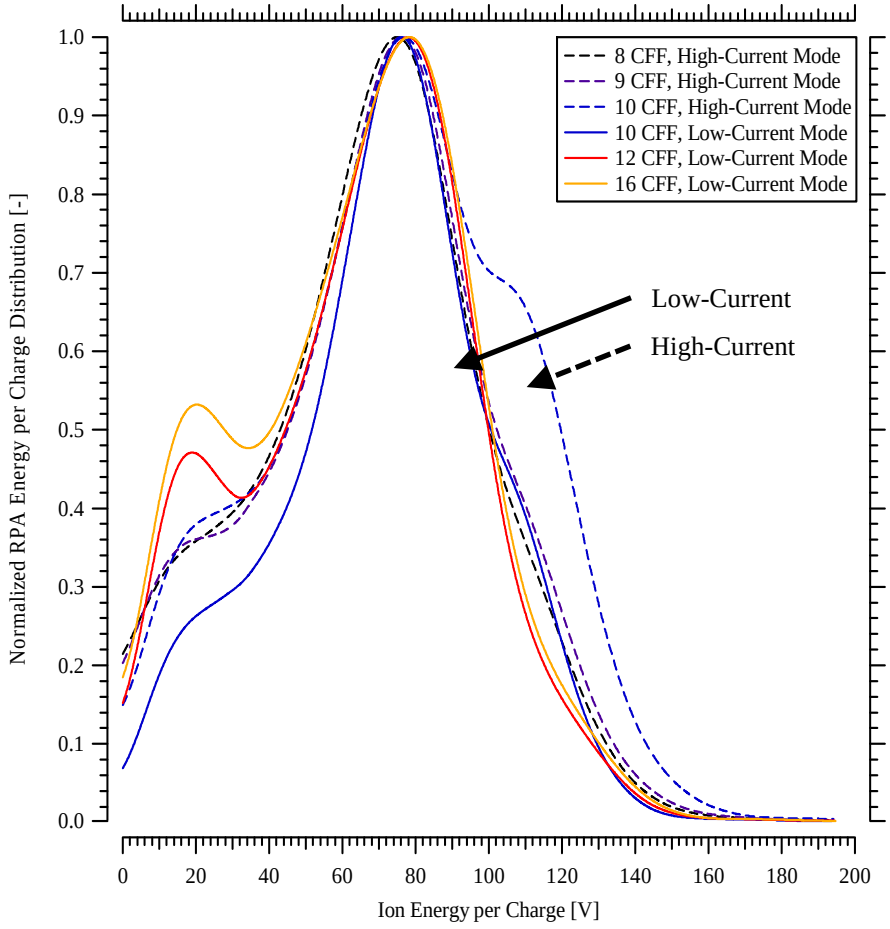

Large Increase in Ion Energy Properties

Background – 4

Past Experiments Reveal Low-Voltage Hall Thruster Mode Transitions

Parameter	Local Oscillation Mode (Low-Current Mode)	Global Oscillation Mode (High-Current Mode)
Discharge Oscillations	• Local spoke perturbations rotate azimuthally in the ExB direction • Small oscillation amplitude, RMS <10% mean discharge current	• Entire channel oscillates in unison, azimuthal spokes absent or negligible. • High oscillation amplitude, RMS >10% of mean discharge current.
Discharge Current	• Mean discharge current consistent with nominal thruster operation	• Elevated discharge current, 5% to 20% higher than local oscillation mode
Plume Shape	• Collimated plume, no center spike feature on thruster centerline	• Collimated plume with center spike on thruster centerline *(center-mount or external cathode)*
Thrust	• Nominal	• Nominal
Performance	• Nominal	• Reduced performance and thrust to power ratio at higher discharge current
Plasma Properties	• Nominal	• Increased electron current to anode

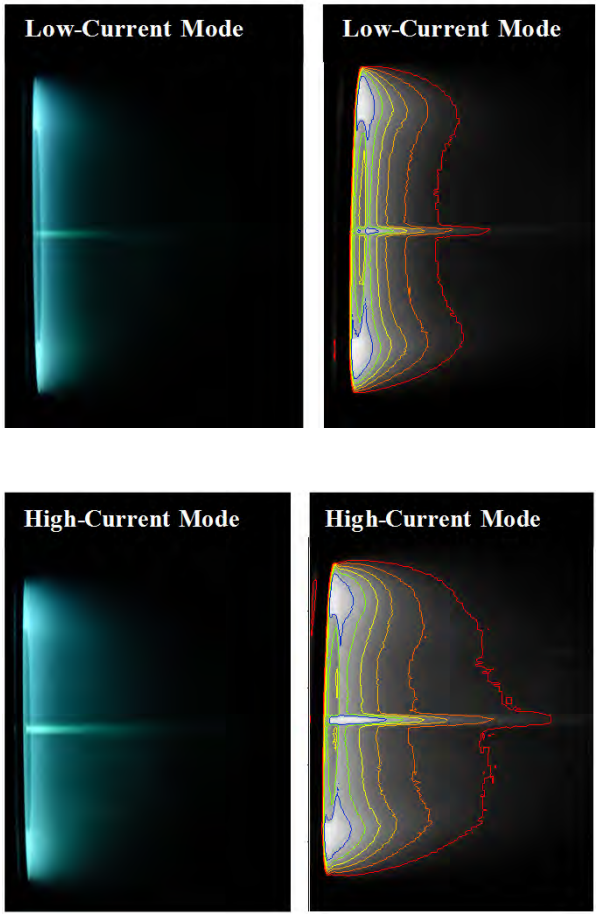

Follow-on Investigations Identify Spoke Oscillations and Transitions at Higher Voltage

Background – 5

Ref. Sekerak et al, AIAA-2013-4116, 2013.

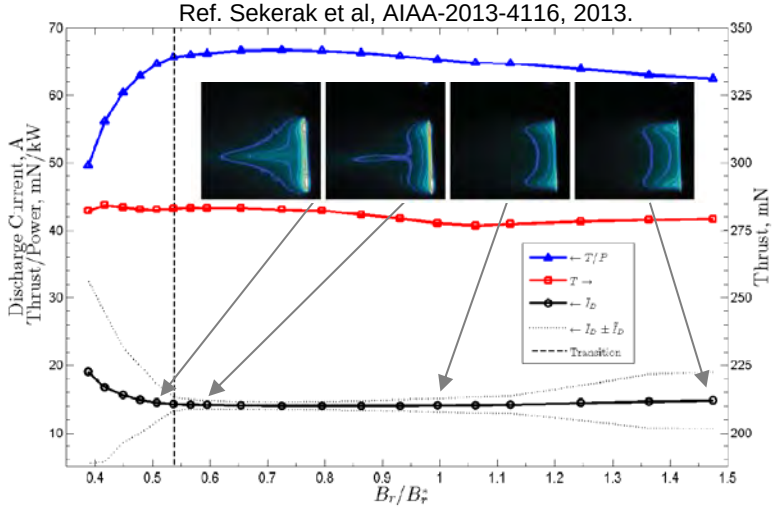

- High-speed imaging analysis to quantify time-resolved azimuthal plasma properties
- Correlate to discharge oscillations and high-speed probe measurements
- Reveals local and global thruster plasma behavior

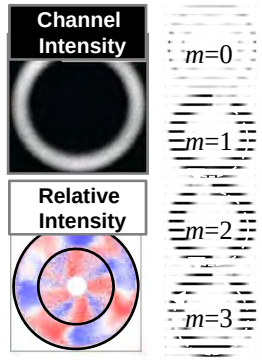

New Understanding Driving Research in Hall Physics and "Anomalous" Electron Transport

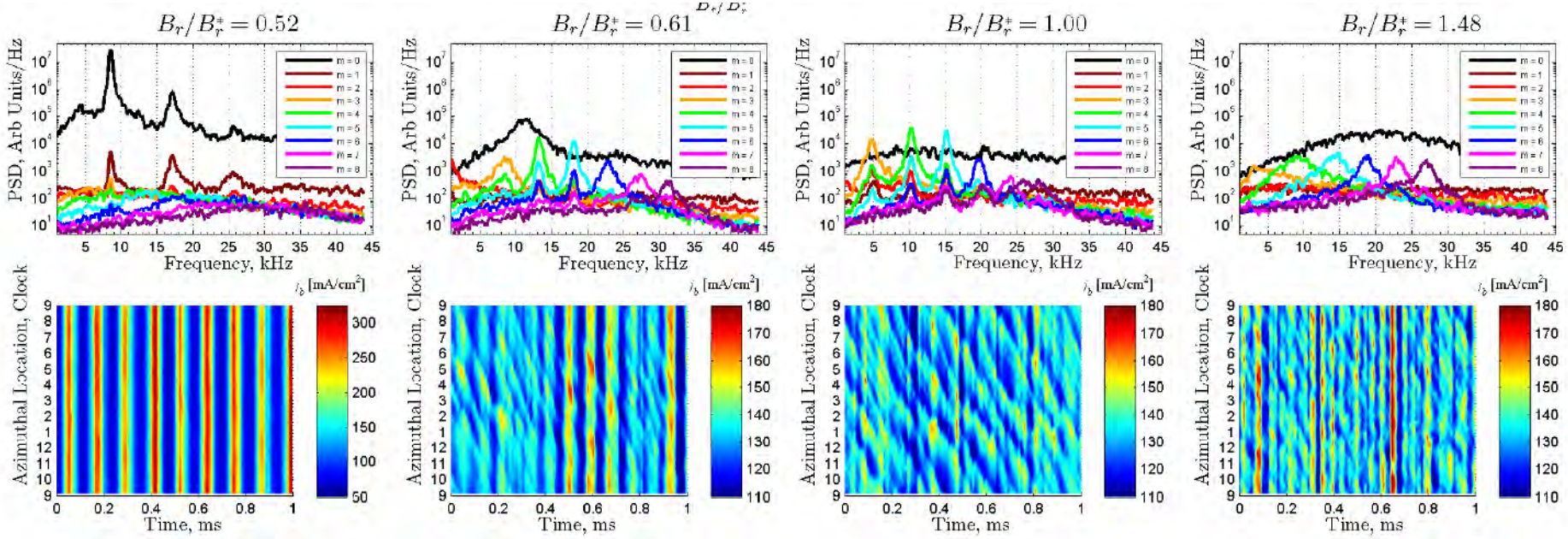

Experimental Apparatus

AFRL SPace Environmental Facility (SPEF)

- 9.1-m diameter stainless steel sphere
- Six 48” diffusion pumps, measured greater than 300,000 L/s on Xe
- Base pressure <1x10^{-6} torr
- Thruster operating pressure ranged from 1.3x10^{-6} to 4.8x10^{-6} torr-xenon at walls

H6 6kW Hall Thruster

- Assess fixed inner, outer electromagnet split, no trim coil
- Evaluate 2 cathode configurations, both <10G at exit
  - Center-mount LaB6, nominal configuration, JPL design
  - External BHC-5000 hollow cathode, outside seperatrix
- Evaluate conditions based on past experiments

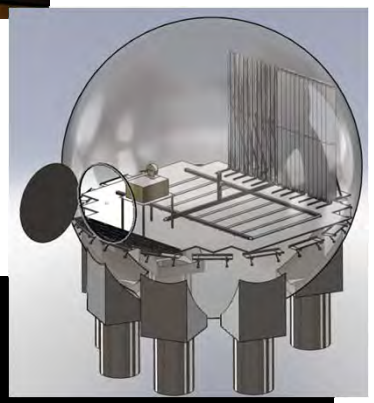

Anode Flow Rate (mg/s)	Cathode Flow Fraction (% Anode)	Discharge Voltage (V)	Electromagnet Current (A)	Electromagnet Current (A)	LaB6 Cathode (Center-mount)	BHC-5000 (External)
10	7	100-200	1.0-5.0	Inner = Outer	Yes	Yes
10	16	100-200	1.0-5.0	Inner = Outer	Yes	Yes
10*	7	100-200	1.0-5.0	Inner/Outer = 1.2	Yes	No
10*	7	100-200	1.0-5.0	Outer/Inner = 1.2	Yes	No
20	7	100-200	1.0-5.0	Inner = Outer	Yes	No
20	12	100-200	1.0-5.0	Inner = Outer	Yes	No

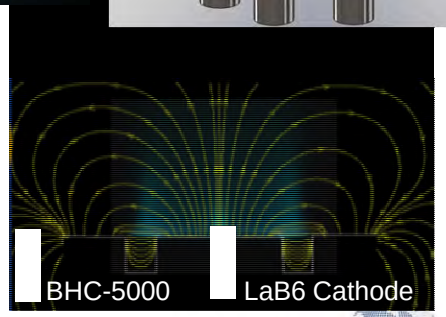

Approach

- Automated monitoring of discharge telemetry at thrust stand waterfall, 100Hz
- Sweep voltage 200V – 100V – 200V, 5V/2sec, average final 1 sec each setting
- Qualitative assessment of thruster & cathode temperatures w/ 4 thermocouples
- All discharge wiring shielded, minimal interference during high oscillations

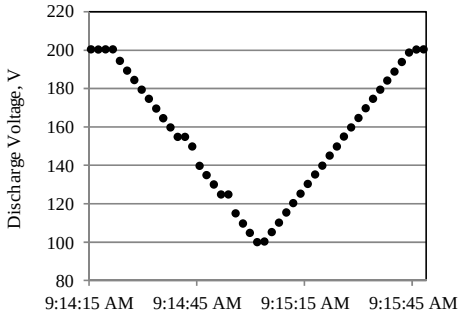

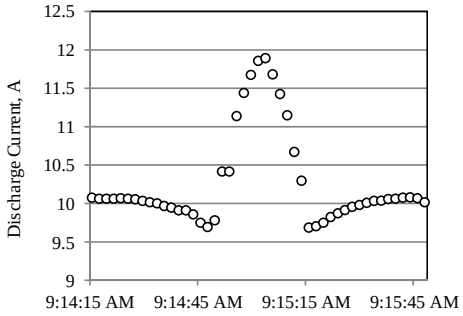

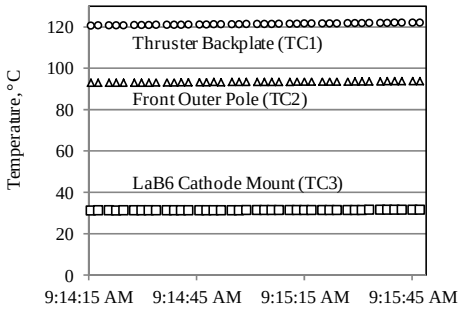

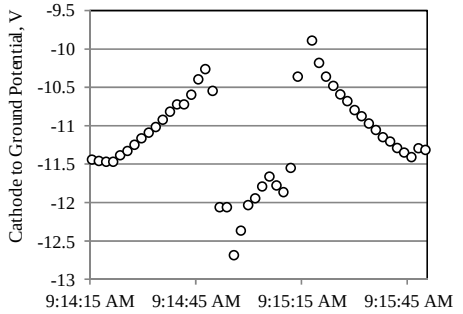

Notes

- Minimal measurement uncertainty in I_d and V_{cg}, <1%
- Minimal change in temperature during scan, approximately 8 degrees C over a full I-V-B map
- Minimal hysteresis in discharge current with sweep direction
- Hysteresis measured in cathode to ground potential near transition
- I-V scan repeatable over multiple days and consistent with full scan up to 600V, 10mg/s

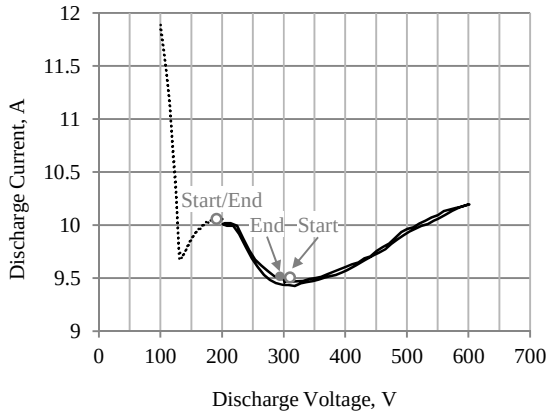

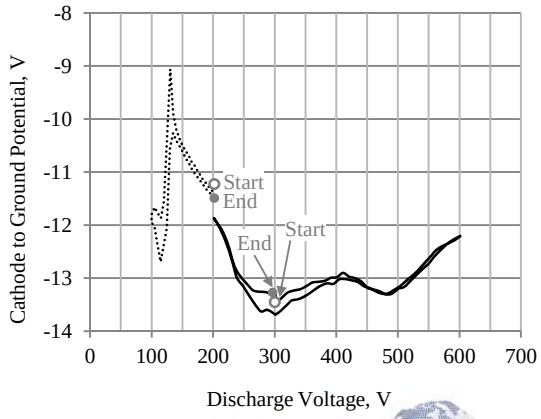

Voltage and Magnetic Field Characterization

10mg/s, Center-mount Cathode, 7% vs 16% CFF

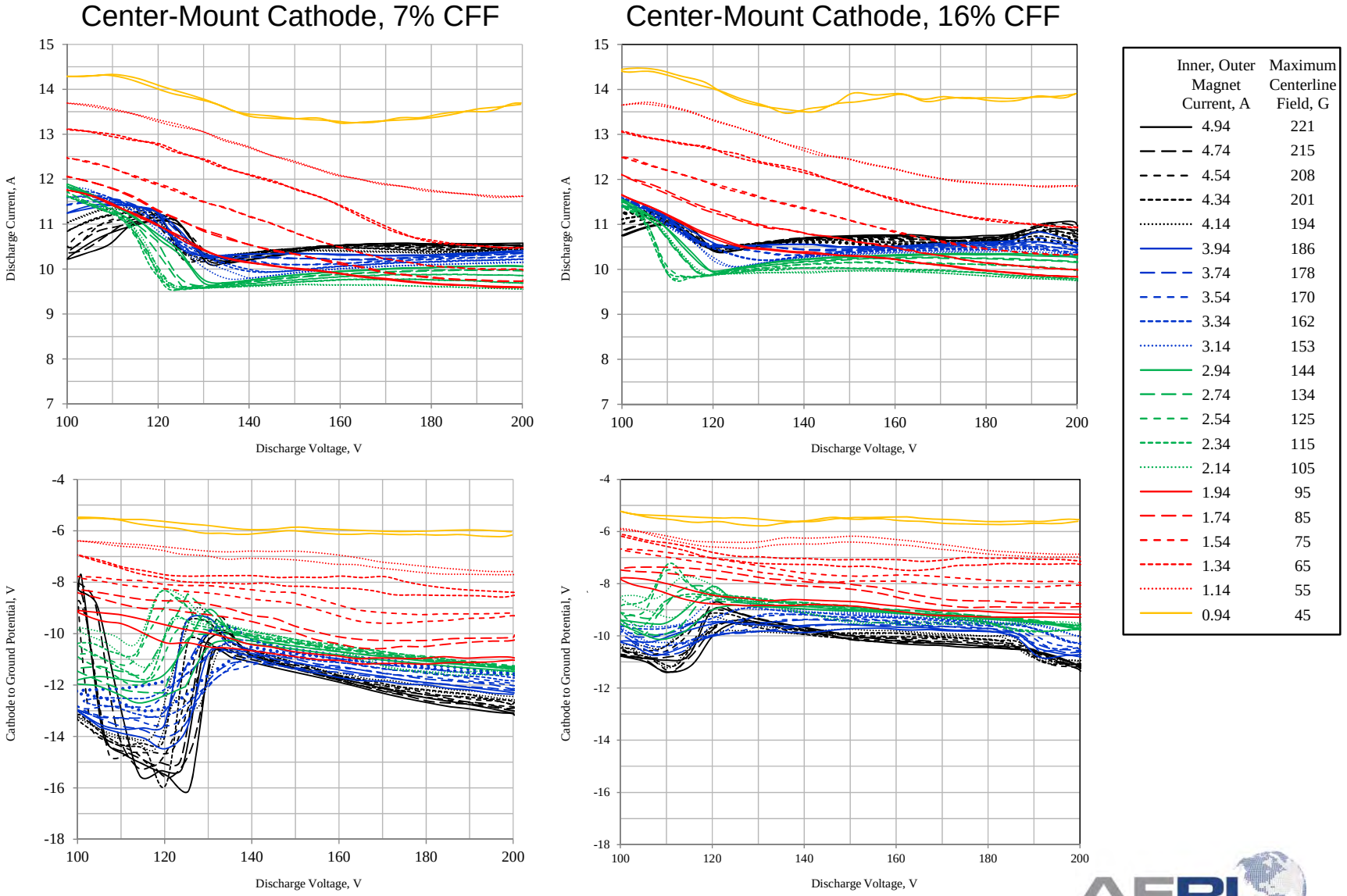

Voltage and Magnetic Field Characterization

10mg/s, Center-mount vs External Cathode, 7% CFF

Center-Mount Cathode, 7% CFF

External Cathode, 7% CFF

Discharge Current, A

Cathode-Ground Potential, V

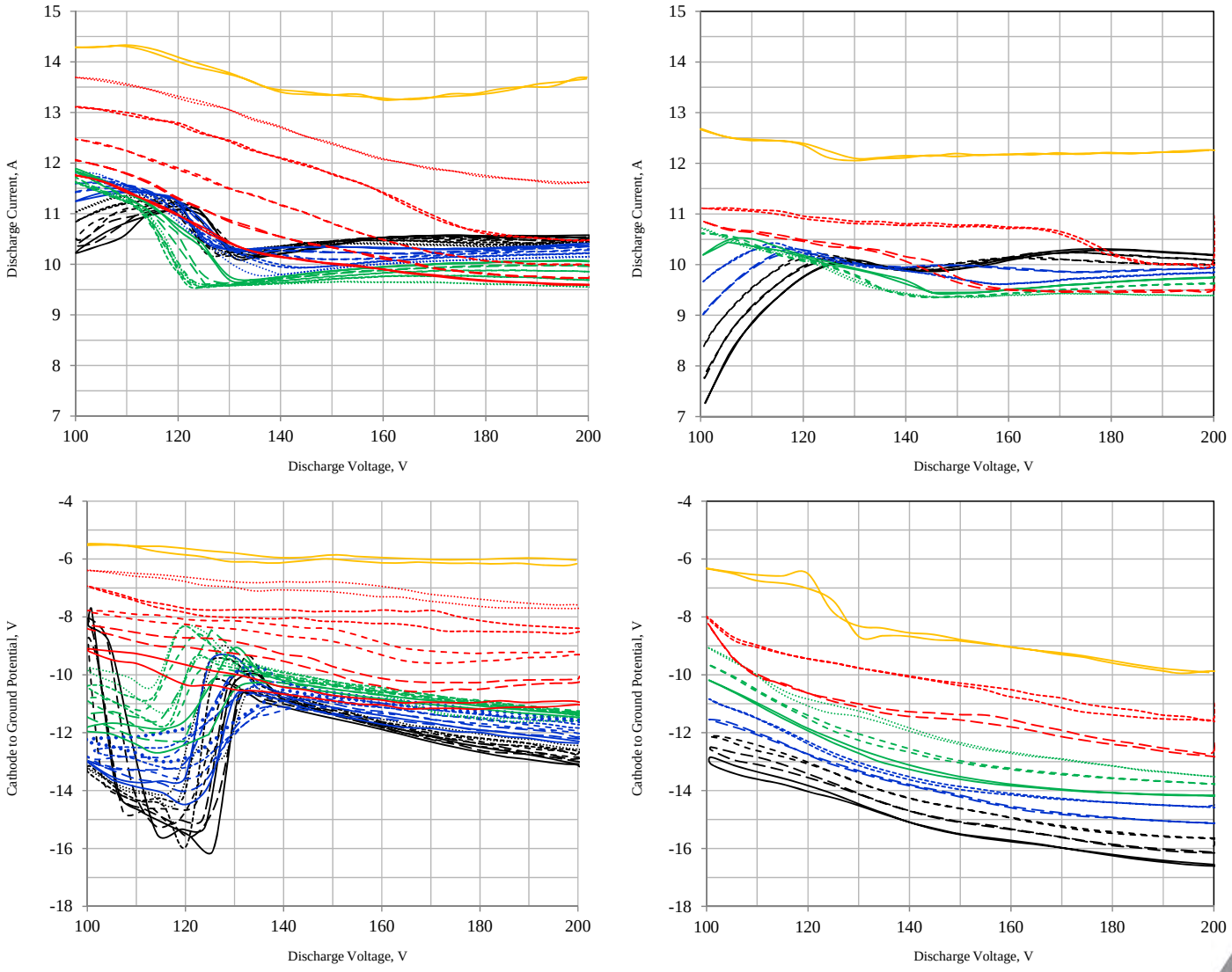

Inner, Outer Magnet Current, A	Maximum Centerline Field, G
4.94	221
4.74	215
4.54	208
4.34	201
4.14	194
3.94	186
3.74	178
3.54	170
3.34	162
3.14	153
2.94	144
2.74	134
2.54	125
2.34	115
2.14	105
1.94	95
1.74	85
1.54	75
1.34	65
1.14	55
0.94	45

Global Thruster Behavior

I-V-B Mapping, 10mg/s, 100V – 600V, 7% CFF

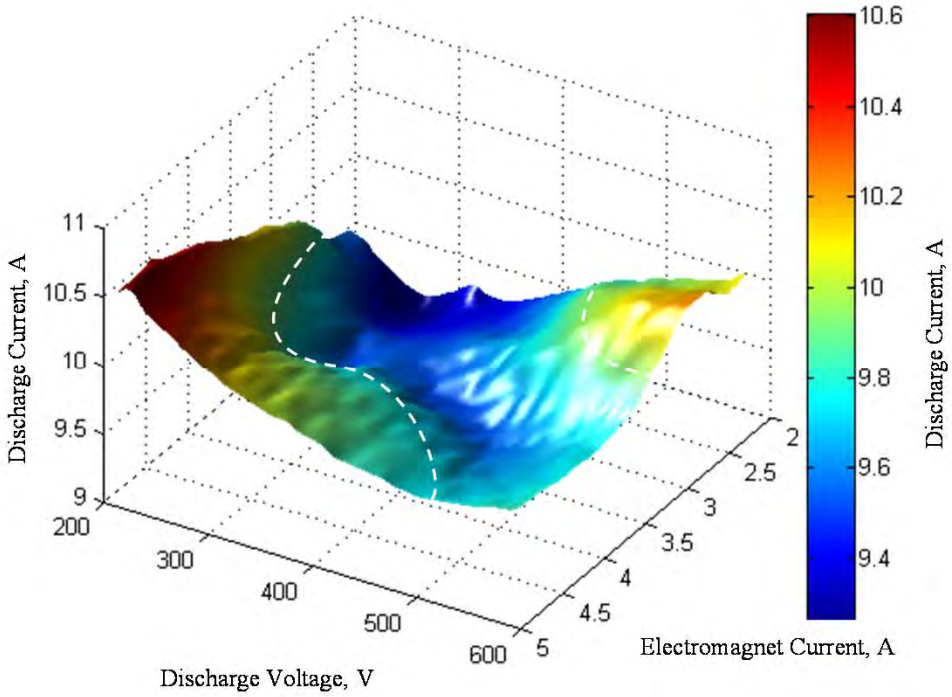

Low-voltage thruster behavior shows significantly higher current above nominal

Full I-V-B map shows global thruster behavior

- Valley from 200V to 600V consistent with past trends (higher B for higher V_d)
- Dashed line shows mode transition region at higher discharge voltages
- Variation in discharge current approx. <10% over full operational envelope
- Lower B expected to trigger mode transition

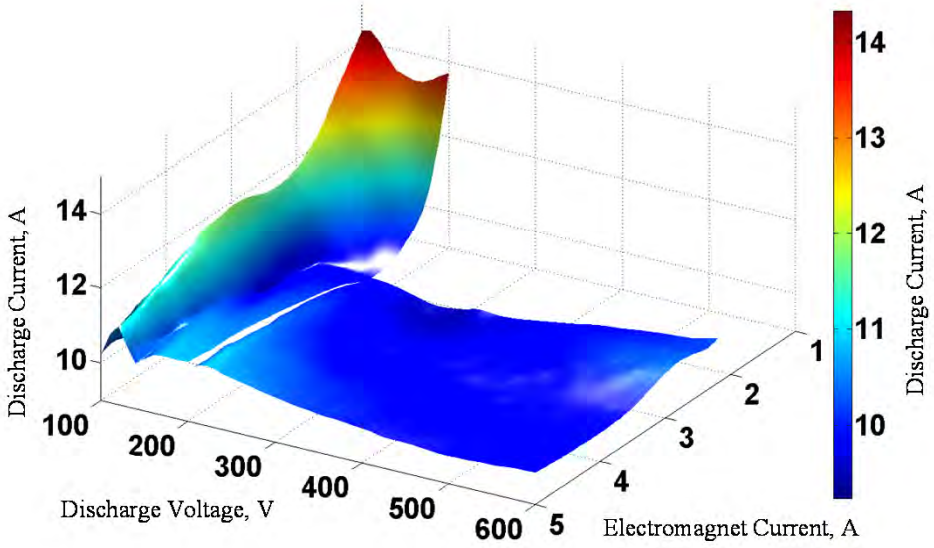

I-V-B Transition Region

100V – 200V, 10 mg/s, Center-Mount vs External Cathode

Center-Mount Cathode

External Cathode

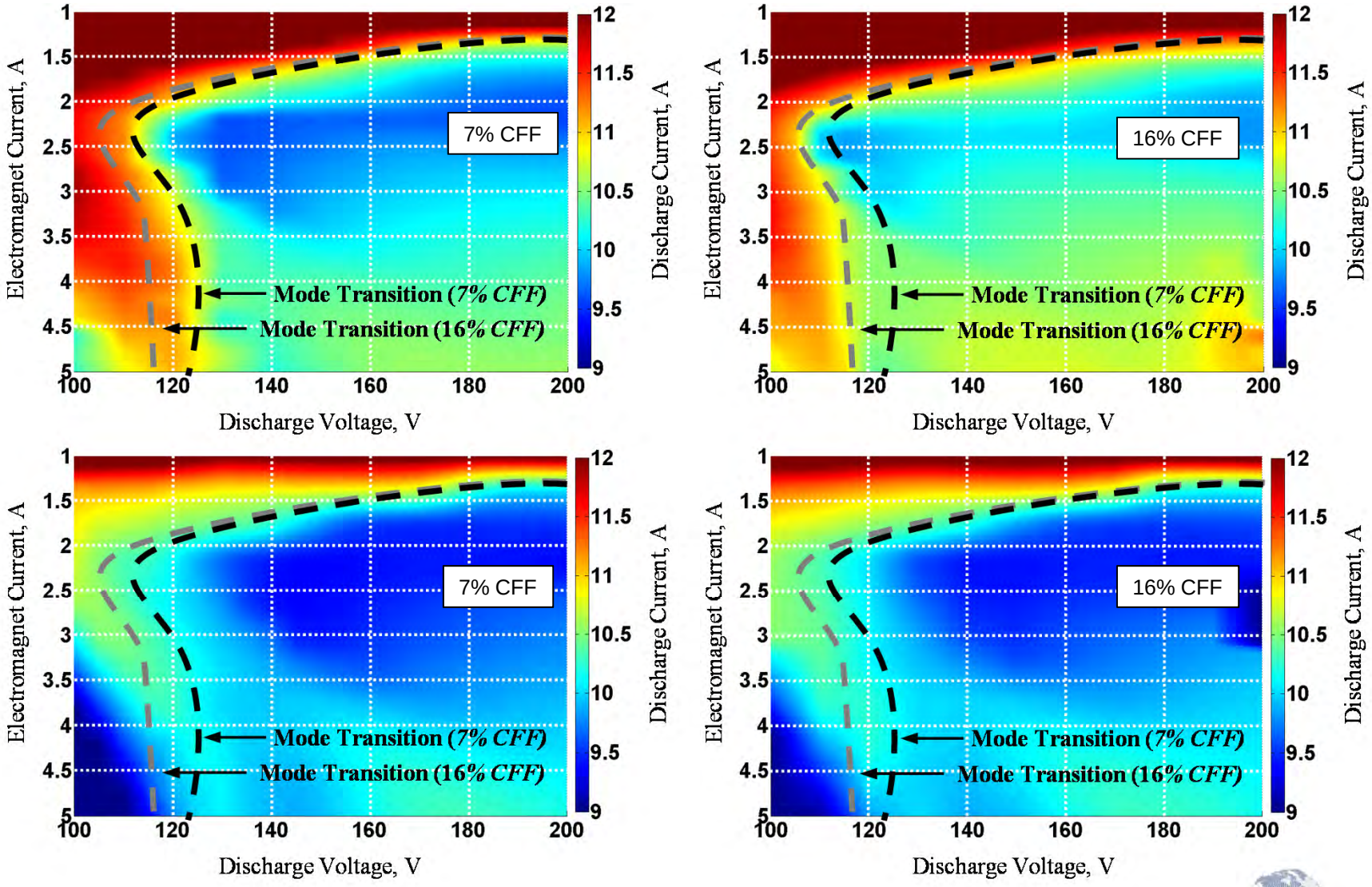

I-V-B Transition Region

100V – 200V, 10 vs 20 mg/s, Center-Mount Cathode

10 mg/s

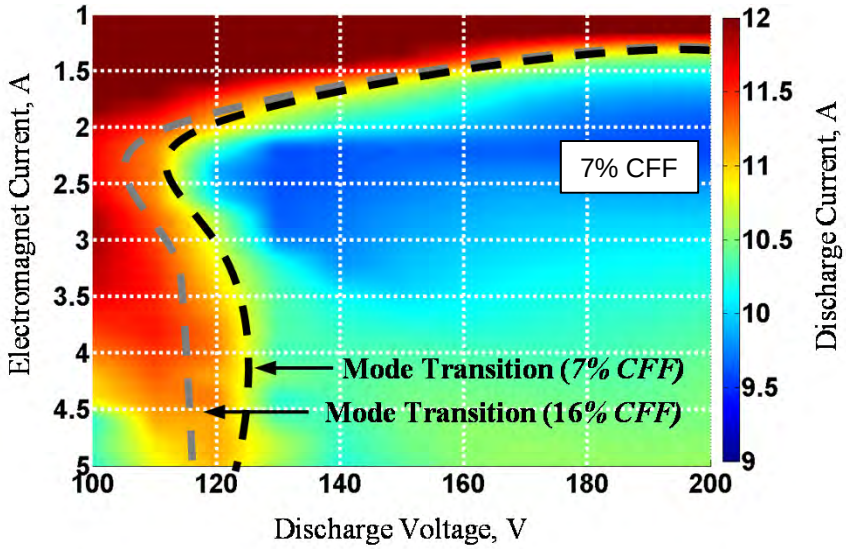

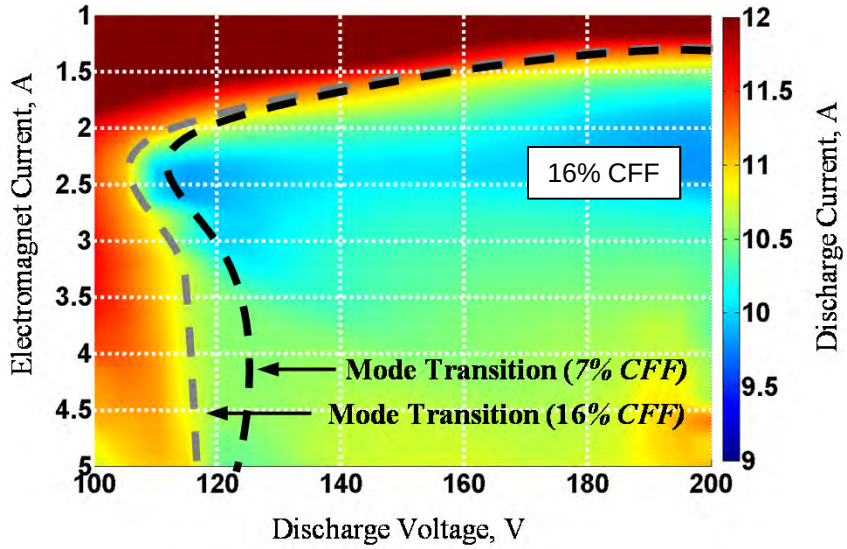

20 mg/s

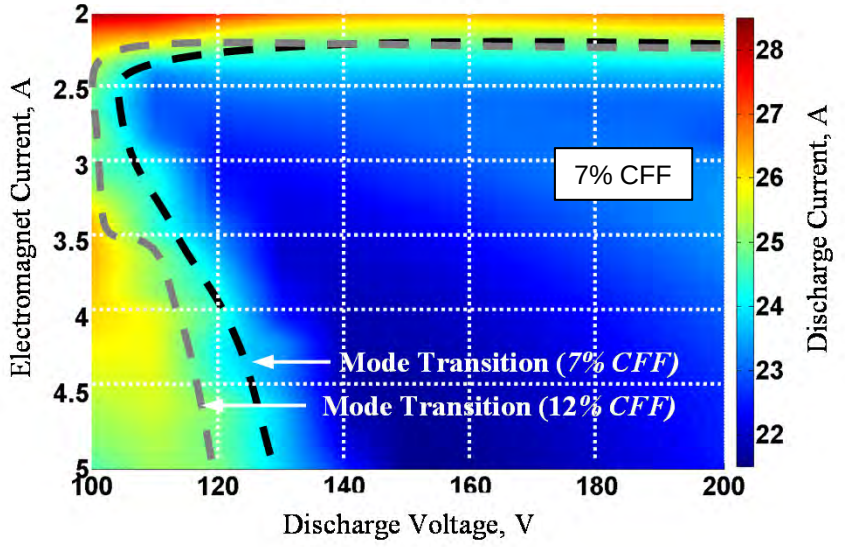

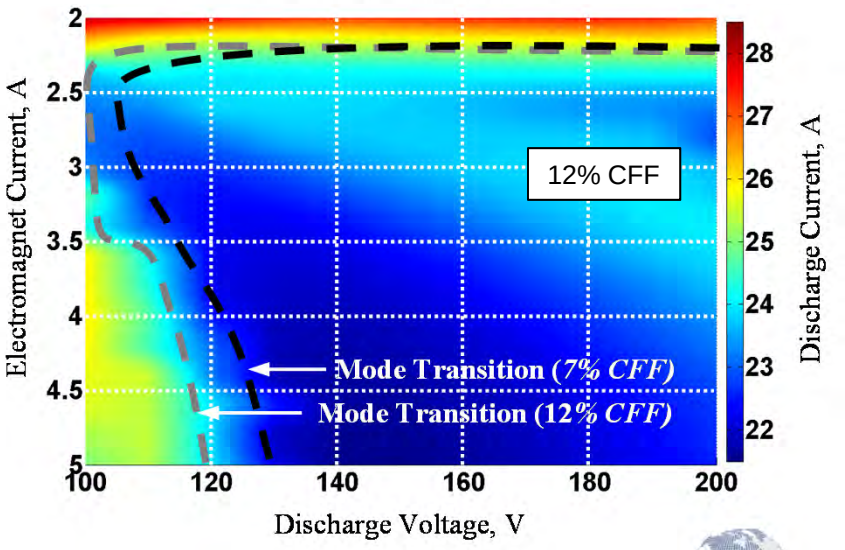

Comparison to Past Experiments

100V – 120V, 10 mg/s, Center-Mount Cathode, 7%-26% CFF

Past Experiment (IEPC-2009-074)

- Mode transition in past data consistent with I-V-B maps
- Maps show region enabling peak T/P in small window of B-field near ~2.5A
- Increased CFF shifts transition to lower discharge voltage
- Minimal change in transition region at low B-field

10 mg/s Anode Flow Condition

- Low-voltage (~120V) or low magnet (1.5-2A) may cause mode transition
- Operating in low-current mode at magnetic field <2A

20 mg/s Anode Flow Condition

- Transition to high-current mode at ~2.2A magnet current across discharge voltage range
- Wide range of magnetic field for high T/P in low-current mode, possibly lower voltage operation

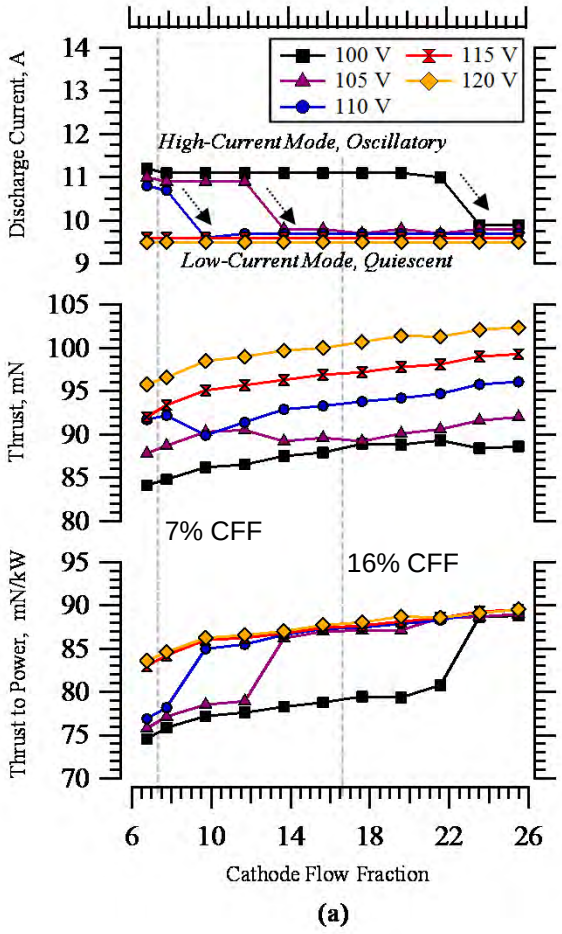

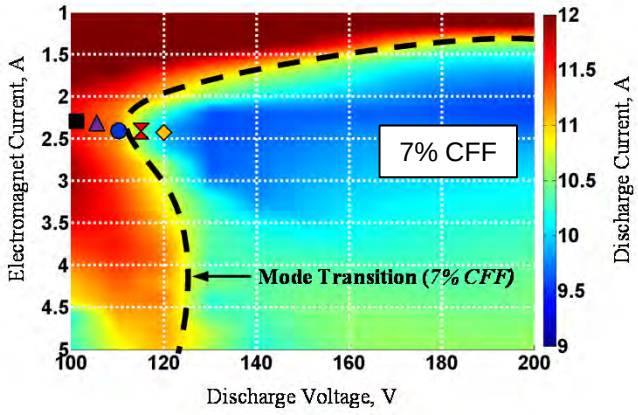

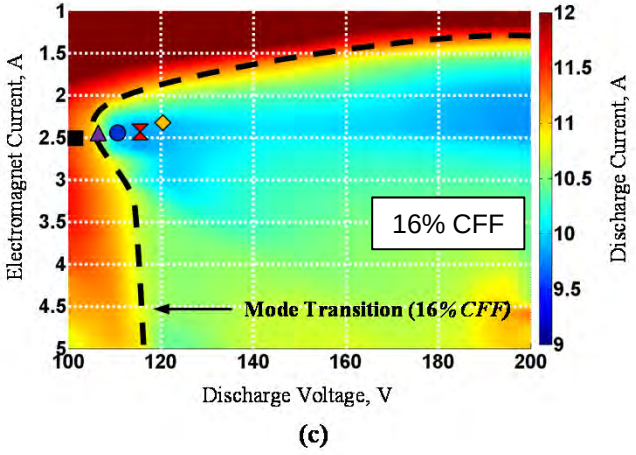

Comparison to Past Experiments

100V – 120V, 20 mg/s, Center-Mount Cathode, 7%-14% CFF

Past Experiment (IEPC-2009-074)

- Mode transition in past data consistent with I-V-B maps
- Maps show region enabling peak T/P in small window of B-field near ~2.5A
- Increased CFF shifts transition to lower discharge voltage
- Minimal change in transition region at low B-field

10 mg/s Anode Flow Condition

- Low-voltage (~120V) or low magnet (1.5-2A) may cause mode transition
- Operating in low-current mode at magnetic field <2A

20 mg/s Anode Flow Condition

- Transition to high-current mode at ~2.2A magnet current across discharge voltage range
- Wide range of magnetic field for high T/P in low-current mode, possibly lower voltage operation

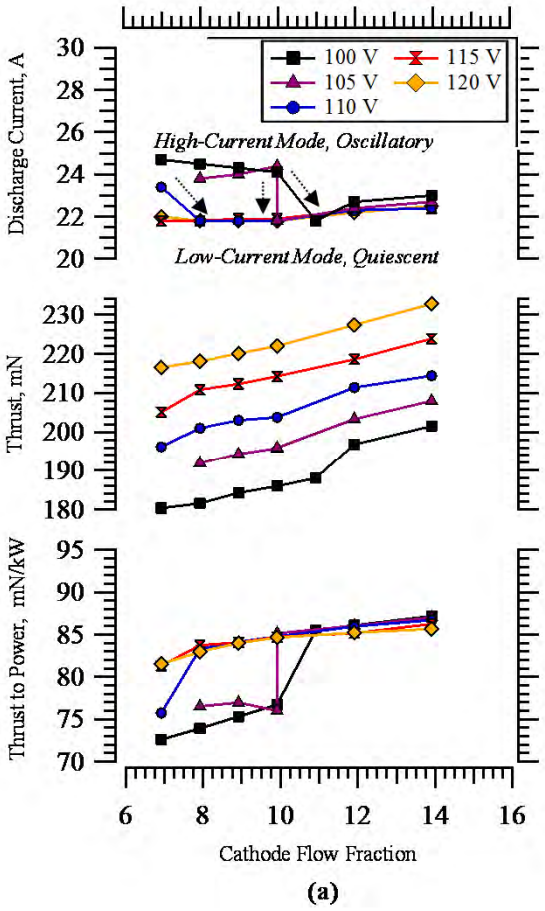

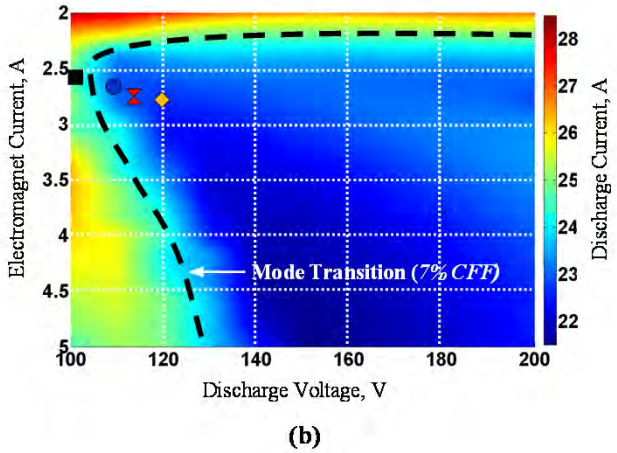

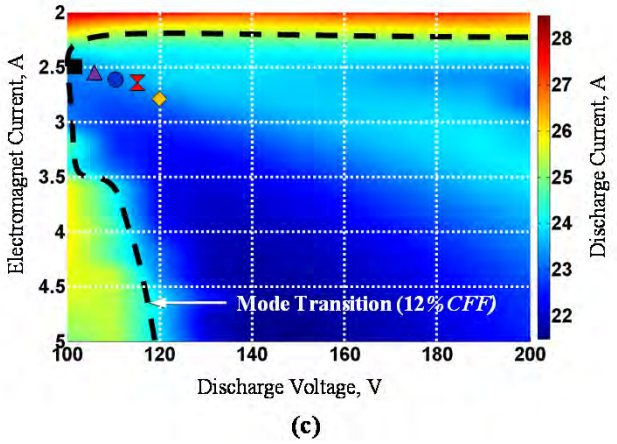

Analysis of Bulk Electron Parameters

100V – 120V, 10-20 mg/s, Center-Mount Cathode, 7% CFF

Center-Mount Cathode, 10mg/s, 7% CFF

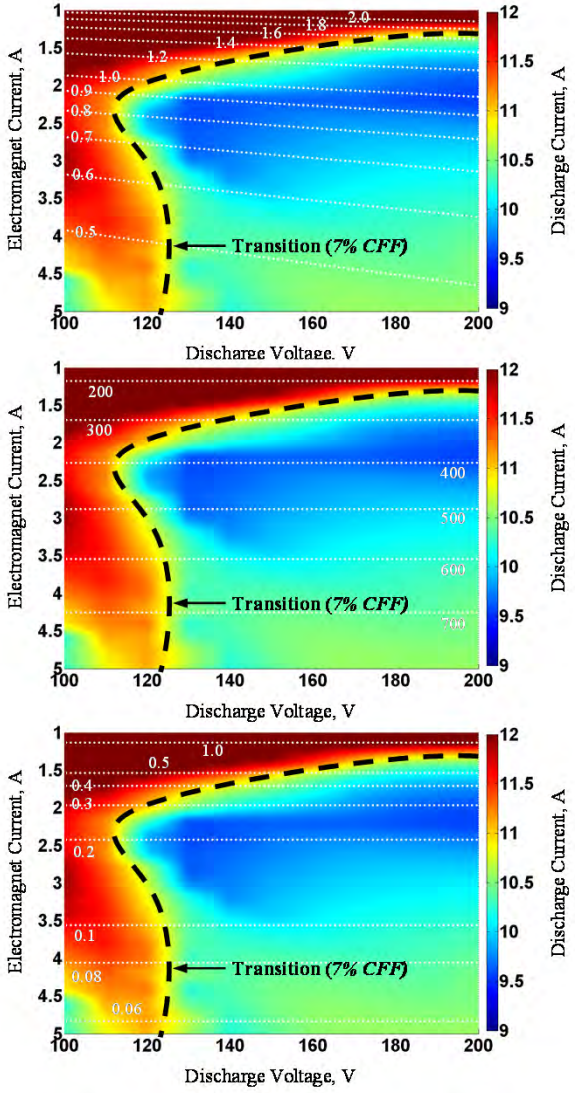

Center-Mount Cathode, 20mg/s, 7% CFF

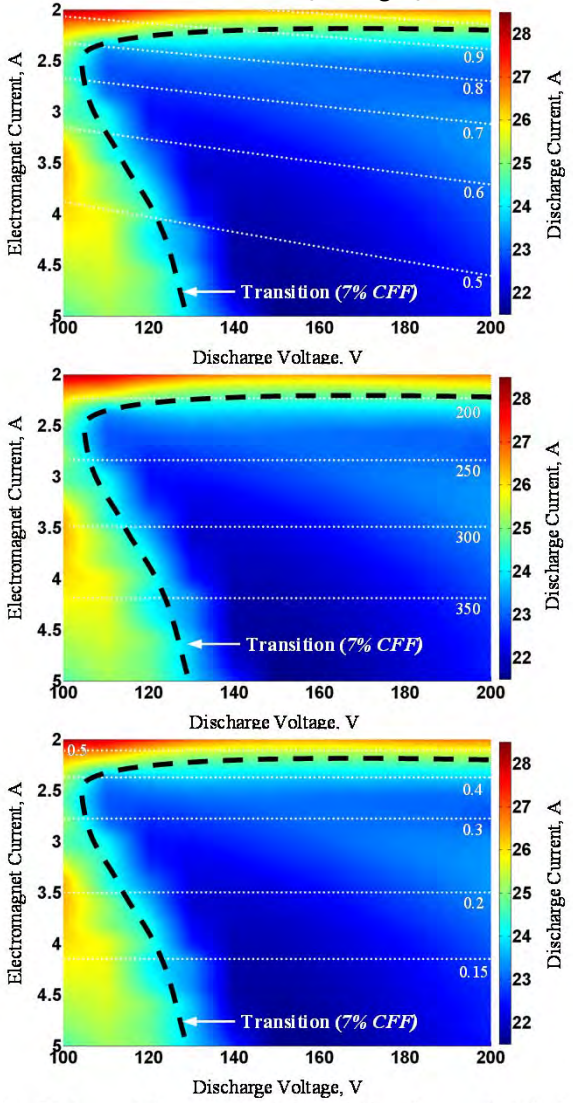

Parameters calculated for:
Electron collision freq. 0.5-1.0x10^7 Hz
Electron temperature 15-20eV

Lines of Constant Electron Gyroradius

- *Range 0.5-2.0 mm*
- *r_e < H6 acceleration length (~10-20mm)*

$$r_e = \sqrt{\frac{k T_e}{m_e}} \frac{m_e}{e B}$$

Lines of Constant Electron Hall Parameter

- *Range 200-700*
- *Expected range based on past internal measurements*
- *Mode transition occurs ~200*

$$\Omega_e = \frac{e B}{\nu_e m_e}$$

Lines of Cross-Field Electron Mobility

- *Range 0.06-1.0* $m^2V^{-1}s^{-1}$
- Mode transition occurs ~0.5 $m^2V^{-1}s^{-1}$
- Significant reduction at mobility increases

$$\mu_{e\perp} = \frac{e}{\nu_e m_e}\left(\frac{1}{1+\Omega_e^2}\right) \approx \frac{\nu_e m_e}{e B_r^2}$$

Summary and Conclusions

- **Analysis of low-voltage I-V-B maps shows mode transitions behavior**
  - Mode transition region consistent with past data at AFRL and UM
  - Maps show region enabling peak T/P in small window of B-field near ~2.5A (~125G)
  - Hysteresis and early transition behavior observed in cathode to ground potential, not in time-averaged discharge current
  - Large I-V-B differences between center-mount and external cathode <130G for low-voltage transition, minimal difference >130V
  - Increased CFF shifted transition to lower-voltage for center-mount cathode, negligible difference for external cathode *(thruster less sensitive to local neutral density or masked by facility interactions?)*
  - Higher anode flow (20mg/s vs 10mg/s) exhibited wider region of B-field for low-current operation at high T/P

- **Analysis of bulk electron dynamics indicates cross-field electron mobility and/or Hall current may be associated with low magnet mode transition**
- **Physics of transition at low voltage more complex, may be combination of ionization/acceleration mechanisms and electron dynamics**
- **Recommend time and spatially resolved plasma measurements of channel and near-field to improve understanding of mode transitions**

BACK-UP

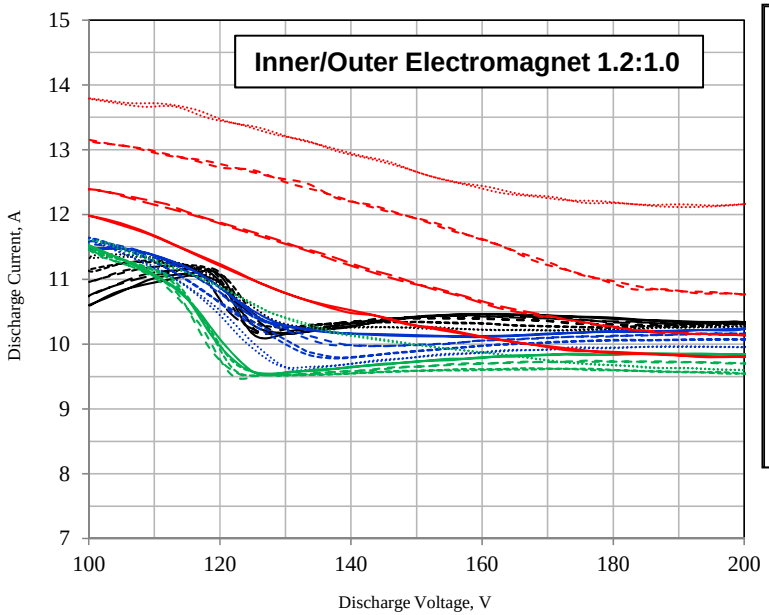

Inner Magnet Current, A	Outer Magnet Current, A
4.98	4.15
4.74	3.95
4.50	3.75
4.26	3.55
4.02	3.35
3.78	3.15
3.54	2.95
3.30	2.75
3.06	2.55
2.81	2.34
2.58	2.15
2.34	1.95
2.10	1.75
1.86	1.55
1.62	1.35
1.38	1.15
1.14	0.95

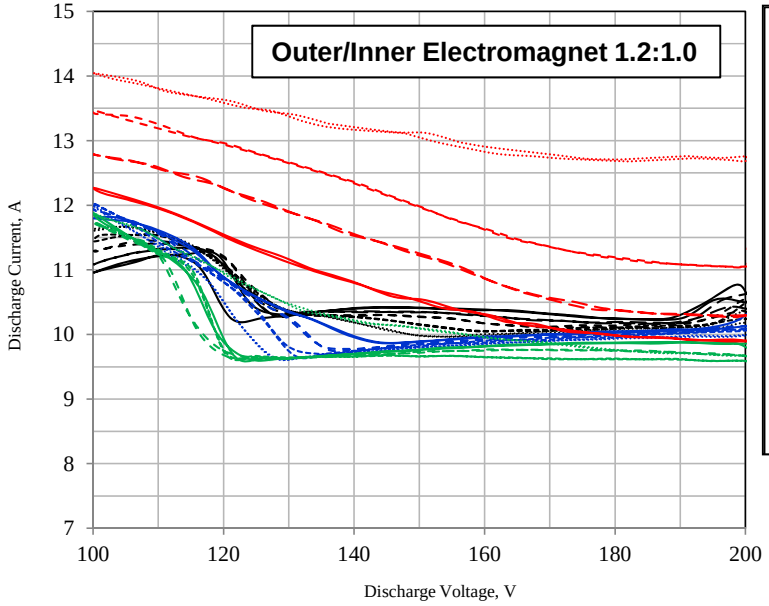

Inner Magnet Current, A	Outer Magnet Current, A
4.15	4.98
3.95	4.74
3.75	4.50
3.55	4.26
3.35	4.02
3.15	3.78
2.95	3.54
2.75	3.30
2.55	3.06
2.34	2.81
2.15	2.58
1.95	2.34
1.75	2.10
1.55	1.86
1.35	1.62
1.15	1.38
0.95	1.14